

SYNTHESIS AND SPECTROSCOPIC STUDIES OF RARE  
EARTH DOPED KNN CERAMIC

A DISSERTATION

SUBMITTED IN PARTIAL FULFILLMENT OF THE REQUIREMENTS

FOR THE AWARD OF THE DEGREE

OF

MASTER OF SCIENCE

IN

APPLIED PHYSICS

Submitted by:

MUSKAN VARSHNEY

2K21/MSCPHY/56

SHREYA SONI

2K21/MSCPHY/44

Under the supervision of

DR. RENUKA BOKOLIA

DEPARTMENT OF APPLIED PHYSICS  
DELHI TECHNOLOGICAL UNIVERSITY  
(Formerly Delhi College of Engineering)

Bawana Road, Delhi 110042

MAY, 2023

## DELHI TECHNOLOGICAL UNIVERSITY

(Formerly Delhi College of  
Engineering) Bawana Road, Delhi-  
110042

CANDIDATE'S DECLARATION

We hereby declare that the project Dissertation titled "Synthesis and spectroscopic studies of rare earth doped KNN ceramic", which is submitted by us to the Department of Applied Physics, Delhi Technological University, Delhi in partial fulfilment of the requirement for the award of the degree of Master of Science is original and not copied from any source without proper citation. This work has not previously formed the basis for the award of any Degree, Diploma Associateship, Fellowship or other similar title or recognition. The work has been communicated in peer-reviewed Scopus indexed conference & journal with the following details:

Title of Paper:

- Conference- Modification of structural, ferroelectric and photoluminescence properties of KNN by  $\text{Er}^{3+}$  incorporation.
- Journal- Energy storage capacity and light upconversion luminescence studies in  $\text{Er}^{3+}$  modified  $\text{K}_{0.5}\text{Na}_{0.5}\text{NbO}_3$  ceramics.

Author names (in sequence as per research paper): Muskan Varshney, Shreya Soni, Ankita Banwal, Renuka Bokolia

Name of Conference: National Seminar on Ferroelectrics and Dielectrics (XXII NSFD-2022)

Name of the Journal: CERAMICS INTERNATIONAL

Conference Dates with venue: 17<sup>th</sup> -19<sup>th</sup> December 2022, Online, Virtual mode

Registration status of the Conference: Done

Status of paper in Journal: Communicated

Date of paper communication: 15 April, 2023

Place: Delhi

Date: 31 May 2023



Muskan Varshney  
(2k21/MSCPHY/56)

Shreya Soni  
(2K21/MSCPHY/44)

DEPARTMENT OF APPLIED PHYSICS  
DELHI TECHNOLOGICAL UNIVERSITY  
(Formerly Delhi College of Engineering)  
Bawana Road, Delhi-110042

CERTIFICATE

We hereby certify that the Project Dissertation titled "Synthesis and spectroscopic studies of rare earth doped KNN ceramic", which is submitted by Muskan Varshney and Shreya Soni, Roll No (s) 2K21/MSCPHY/56 and 2K21/MSCPHY/44, Department of Applied Physics, Delhi Technological University, Delhi in partial fulfilment of the requirement for the award of the degree of Master of Science, is a record of the project work carried out by the students under my supervision. To the best of my knowledge, this work has not been submitted in part or full for any Degree or Diploma to this University or elsewhere.

Place: Delhi

Date: MAY 2023

Dr.Renuka  
Bokolia

SUPERVISOR

ASSISTANT PROFESSOR

## Abstract

The lead-free ceramics potassium sodium niobate, KNN, ( $\text{K}_{0.5}\text{Na}_{0.5}\text{NbO}_3$ ) were synthesized by solid-state reaction method to study the effect of rare earth ions ( $\text{Er}^{3+}$ ) on structural, ferroelectric and optical properties. In order to explore how temperature affects crystal formation, the undoped KNN was calcined at various temperatures ranging from 700 to 900°C. The powder X-ray diffraction pattern revealed the absence of secondary phases, confirming the formation of pure KNN phase, which was calcined at 900°C for 3h and then sintered at 1100°C for 3h to form a single-phase perovskite crystal with orthorhombic geometry. The XRD spectra of  $\text{Er}^{3+}$  doped KNN showed no extra phases confirming the complete diffusion of  $\text{Er}^{3+}$  ions into the host lattice. The FTIR band at 486  $\text{cm}^{-1}$  & 720  $\text{cm}^{-1}$  showed the formation of a perovskite structure. The PL emission spectra at room temperature of sintered  $\text{Er}^{3+}$  doped KNN pellets at an excitation wavelength of 488 nm and 980 nm were analyzed. In emission spectra, strong green emission bands (528 and 549 nm) and somewhat faint red emission bands (662 nm) were found. The intensity of PL emission spectra using 980 nm wavelength was far much greater than 488 nm, and in the analyses of the effect of power of radiation, it was found that photoluminescence observed is a two-photon phenomenon. The ferroelectric PE loop at room temperature showed decent shapes with good remnant polarization. The energy storage capacity was calculated using the P-E loop; found to have increased from 52.7% for undoped KNN to 67.21% for KNN with optimal erbium concentration, i.e.,  $x=3$ . KNN has excellent inherent piezoelectric capabilities, and by combining its optical and ferroelectric properties, this type of material may also have potential use as a multifunctional device.

## Acknowledgement

We want to start by thanking our supervisor, Dr Renuka Bokolia, for allowing us to work on the structural properties of ferroelectric ceramic KNN. This endeavour would not have been possible without her leadership and unwavering support. We value her valuable time, as well as her insights and suggestions. We also thank Ms Ankita Banwal for fostering a positive work environment and sharing her valuable research experience. We wish to move forward with the various aspects we learned while writing, and we sincerely appreciate their patience in editing our manuscripts. Their combined research strategy kept the spirit of exploration alive for this dissertation. We are also appreciative to our parents and friends for their emotional support, which allowed us to complete this dissertation thesis.



Muskan Varshney  
(2k21/MSCPHY/56)

Shreya Soni  
(2k21/MSCPHY/44)

## **CONTENTS**

- 1. CHAPTER 1 INTRODUCTION**
  - 1.1. Definition and Classification of Photoluminescence
  - 1.2. Photoluminescence
    - 1.2.1 Downconversion luminescence
    - 1.2.2 Upconversion luminescence
  - 1.3. Upconversion Mechanism
  - 1.4. Upconversion Materials
  - 1.5. Luminescent lifetime
  - 1.6. Ferroelectrics
    - 1.6.1. Electrical properties of ferroelectrics
    - 1.6.2. Photoluminescence studies of ferroelectrics
  - 1.7. Rare earth ions
    - 1.7.1. Er<sup>3+</sup>
    - 1.7.2. Pr<sup>3+</sup>
    - 1.7.3. Yb<sup>3+</sup>
  - 1.8. Host selection
- 2. CHAPTER 2 LITERATURE REVIEW**
  - 2.1 Lead-free KNN ceramic
  - 2.2 Scope of Work
- 3. CHAPTER 3 FABRICATION AND CHARACTERIZATION**
  - 3.1. Solid State Reaction Method
  - 3.2. Sample Preparation
  - 3.3. Characterization
    - 3.3.1. Structural characterization- XRD
    - 3.3.2. Chemical characterization- FTIR
    - 3.3.3. Optical characterization- PL
    - 3.3.4. Electrical characterization- PE
- 4. CHAPTER 4 EXPERIMENTAL RESULTS**
  - 4.1 X-Ray Diffraction
  - 4.2 Visible Downconversion Photoluminescence (PL)

4.3 Upconversion Luminescence (UCL)

4.4 Influence of Pump Power on UCL

4.5 Time Decay Analysis

4.6 Fourier Transform Infrared Spectroscopy (FTIR)

4.7 Ferroelectric Properties

4.7.1 PE Loop Analysis

4.7.2 Energy Storage Capacity

**5. CHAPTER 5 CONCLUSION**

**6. REFERENCES**

**7. APPENDICES**



## List of Figures

Figure 1 Types of Luminescence .....	2
Figure 2 Upconversion Mechanism .....	4
Figure 3 Schematic Diagram of Synthesis Process .....	16
Figure 4 (a-e) XRD spectra of pure KNN ceramic calcined at different temperatures (T=700 °C to 900°C).....	21
Figure 5(a) Xrd Spectra of KNN:xEr (x=0,1,2,3,4) sintered at 1100oC (b) XRD spectra displaying peak shifting.....	22
Figure 6 Visible Down Conversion Photoluminescence of KNN:xEr x=1,2,3,4 .....	23
Figure 7 a)Plot of Upconversion luminescence using source wavelength 980nm of KNN:xEr (x=1,2,3,4) b) Plot of intensity vs erbium ion concentration c) Energy level diagram of Erbium.....	25
Figure 8 The emission spectra of upconversion (UC) with increasing pumping power for different concentrations of dopants. ....	27
Figure 9 Log-log plot of KNN:xEr (x=1,2,3,4) ceramic. ....	28
Figure 10 Time decay curve of KNN:xEr ceramic .....	29
Figure 11 a) FTIR spectra of KNN ceramic with varying Er <sup>3+</sup> weight percentage. (b) Variation of FTIR mode with erbium content. ....	30
Figure 12 Hysteresis loop of KNN ceramic a)Pure KNN with zero erbium doping b) KNN with x=3wt% Er .....	31

## List of Table

Table 1: PE dynamics of KNN: xEr (x = 0 and 3) for various electric fields.

### List of symbols, abbreviations

<b>Symbol/Abbreviation</b>	<b>Meaning</b>
<b>PL</b>	Photoluminescence
<b>UCL</b>	Up-conversion Luminescence
<b>XRD</b>	X-ray Diffraction
<b>FTIR</b>	Fourier Transform Infrared Spectroscopy
<b>PE</b>	Polarization - Electric Field
<b>GSA</b>	Ground State Absorption
<b>ESA</b>	Excited State Absorption
<b>MPR</b>	Multi-Phonon Relaxation
<b>ET</b>	Energy Transfer
<b>KNN</b>	Potassium Sodium Niobate ( $K_{0.5}Na_{0.5}NbO_3$ )
<b>Er</b>	Erbium
<b>Yb</b>	Ytterbium
<b>Sm</b>	Samarium
<b><math>\eta</math></b>	Energy Storage Efficiency

## CHAPTER 1

### INTRODUCTION

#### 1.1 DEFINITION AND CLASSIFICATION OF LUMINESCENCE

Wiedemann introduced the term "luminescence" in 1888. Luminescence should not be confused with incandescence, as the two are entirely different[1]. Luminescence is a cold body radiation emitted in the form of photons without any externally applied heat. Instead of heat, many external exciters in energy can be used, like photons, chemical reactions, subatomic motions, electrons, stress etc. Luminescence includes the visible region (380-780 nm) of the emission spectrum and the ultra-violet and infrared region. The human eye is active in the 380-780 nm wavelength range and most responsive around 555 nm wavelength. So, commercial phosphors are used to emit light in this band of wavelengths[2].

Luminescence is classified based on its lifetime or luminescent duration; shorter than  $10^{-8}$  s is termed fluorescence, while longer luminescence is termed phosphorescence. In quantum theory, when a substance emits light during fluorescence, the transitions occur from a specific excited state called the singlet state. In this state, the electron's spin direction remains the same. However, there are certain conditions where a spin flip can occur, creating a lower excited state called the triplet state. This process is known as phosphorescence[3].

The critical point to note is that transitions from the triplet excited state are not allowed according to the selection rules in quantum theory. As a result, the electron in the triplet state has to wait for a relatively long time until its spin flips back. This waiting period causes phosphorescence to have lower intensity compared to fluorescence. Additionally, even after removing the excitation source, phosphorescence can continue for a longer time because the electron takes time to return to its original state. Further, fig.1 tabulates

the various forms of luminescence depending on the condition of excitation that enables it. This dissertation thesis discusses photoluminescence from solids[4].

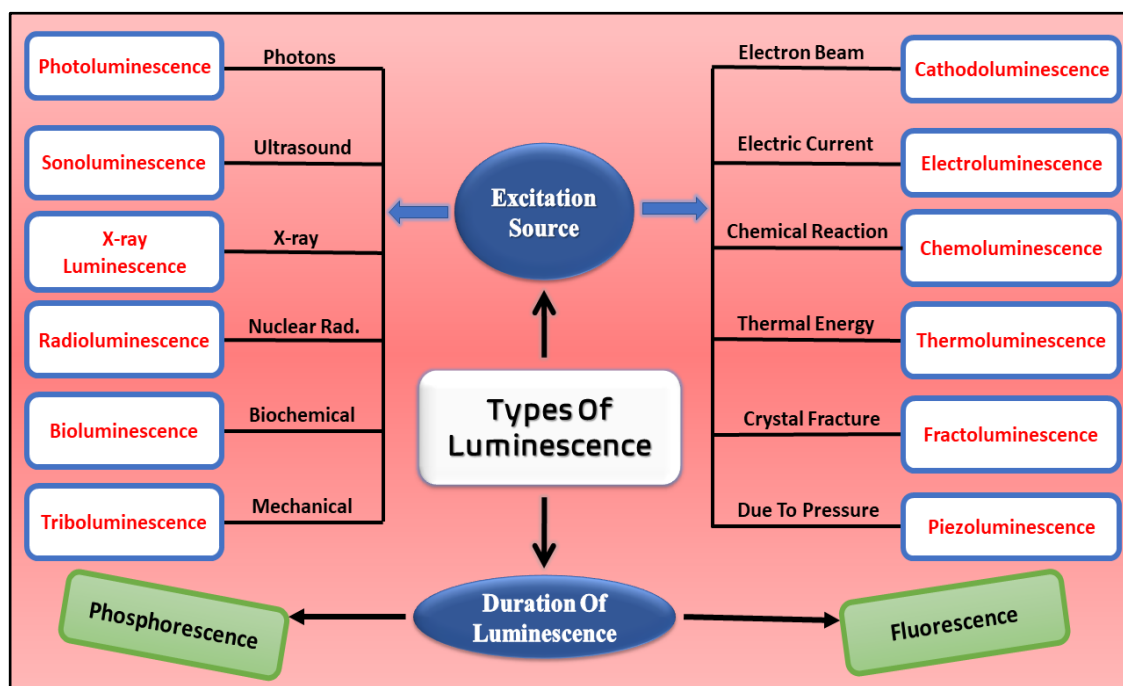


Figure 1 Types of Luminescence

## 1.2 PHOTOLUMINESCENCE

Photoluminescence is a process where light is emitted from any matter upon excitation by photons. The method includes various routes to re-radiate the photons, such as light emission, energy transfer and absorption. Among the mentioned routes, absorption occurs between ground and excited energy levels, while energy transfer occurs only between excited energy levels. Luminescence is only observed when there is absorption of photons. Photon absorption occurs either at the luminescent centre or at any place in the host lattice. If absorption takes place at the luminescent centre, there is direct emission. But if it is at any other site in the host lattice, energy transfer occurs to the luminescent centre so that emission can occur.

Based on the energy of the photon emitted during photoluminescence, it is classified into two. One is down-conversion, and the other is up-conversion.

### 1.2.1 DOWN-CONVERSION LUMINESCENCE

As mentioned, photoluminescence is an emission of photons upon excitation via incident photons. High-energy photons are inefficiently absorbed; thus, multiple photons of lower energy are emitted. The emission is termed down-conversion when emitted photons are of lower energy than the incident photons. Down-conversion is also known as Stokes emission. The energy is lost via various non-radiative emissions, like changes in bond length due to lattice relaxation. The difference between energies of the incident photon and lower energy emitted photon is termed as Stokes shift.

### 1.2.2 UP-CONVERSION LUMINESCENCE

Upconversion luminescence is the luminescence in which higher energy photons are emitted. It implies that more than one photon is absorbed to emit one photon. The energy of more than one incident photon combines to emit higher energy photons. This Upconversion emission is also called anti-Stokes emission, as the lower wavelength photons are emitted during this process. The difference in energies of incident and emission photons is referred to as anti-Stokes shift[5].

### 1.3 UPCONVERSION MECHANISM

This section will explain the Upconversion mechanism in detail. Upconversion involves basic processes: ground state absorption (GSA), excited state absorption (ESA), energy transfer, multi-phonon relaxation and radiative emission.

The incident photon is absorbed by the ground state (GSA); through this energy absorption, electrons reach an excited energy level ( $E_1$ ). GSA is the most uncomplicated process where the activator absorbs energy. If there is a simple radiative emission only after GSA, the luminescence will be downconversion, i.e., a lower energy photon will be emitted. But for upconversion, excited state absorption takes place, meaning another photon is absorbed by the excited state to further excite the electrons to higher energy levels ( $E_2$ ) as shown in fig. 2(a). The radiative emission from energy level  $E_2$  will result in emission photons having greater energy than the incident photons. The mechanism of upconversion is not as simple as it seems, as many non-radiative emissions are involved, which seems to cause a loss of energy. This non-radiative emission includes multi-phonon relaxation. When the electrons are excited to higher energy levels, they often reach short-lived energy levels. These energy levels are not stable enough to cause a radiative de-

excited directly to the ground state, which is crucial to observe an upconversion luminescence. So, these higher excited energy levels reach much more stable excited states by (MPR) multi-phonon relaxation. It is the de-excitation of electrons in the host lattice by losing energy in the form of phonons or lattice vibrations.

There is another mechanism of upconversion where sequential absorption of incident photons takes place, intending two or more incident photons are absorbed simultaneously. In this case, a sensitizer ion is used, which helps in populating the metastable state of the activator ion as shown in fig.2(b). The role of a sensitizer ion is it absorbs a photon, then electrons reach an excited state, and it relaxes and reaches the ground state by transferring the absorbed energy to the activator ion. This helps in the overpopulation of metastable state ( $E_2$ ) in activator ion, which radiatively de-excites and releases photons of higher energy (anti-stokes shift). This energy transfer acts as a catalyst to the upconversion process and also increases the intensity of luminescence observed. The most commonly used sensitizer is ytterbium to activator ion erbium. It should be noted that GSA, ESA only occurs when the energy of an incident photon is comparable to the energy difference between  $E_0$ ,  $E_1$  and  $E_2$ , and energy transfer takes place when the energy difference of  $S_0$  and  $S_1$  of sensitizer ion should be comparable to the energy difference between  $E_1$  and  $E_2$ .

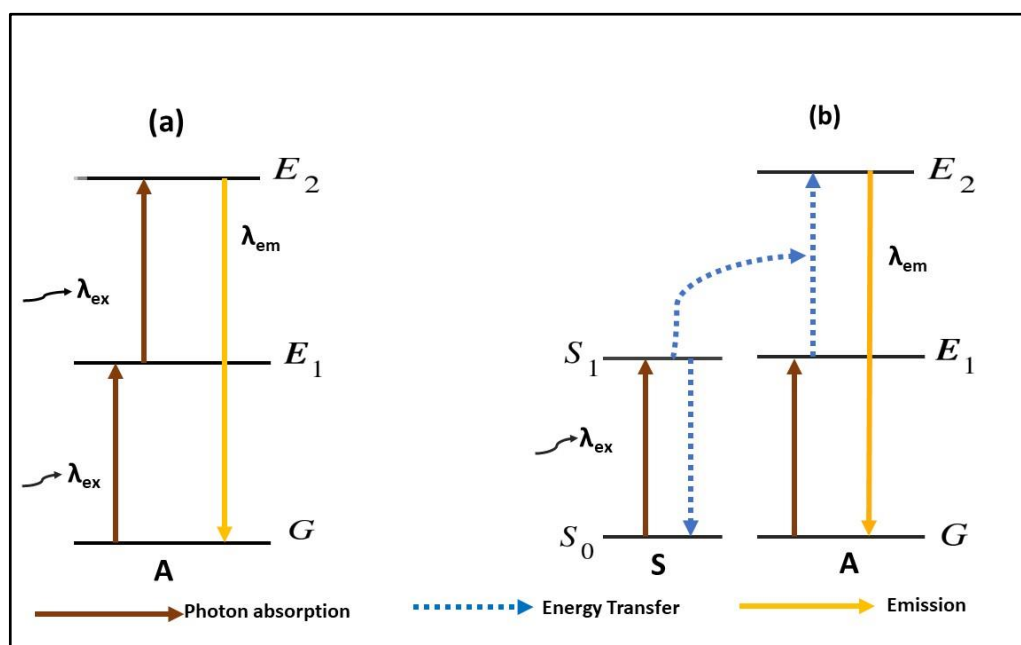


Figure 2 Upconversion Mechanism

#### 1.4 UPCONVERSION MATERIALS

Upconverter materials can be broadly classified as lanthanide-based and organic upconverter materials. Lanthanide-based upconverter materials are known for their high efficiency and excellent photostability, making them ideal for applications in bioimaging and photovoltaics. These materials typically consist of rare earth ions such as erbium, ytterbium, and thulium embedded in a host matrix. Lanthanides comprised of elements from atomic number 57, i.e., lanthanum, to atomic number 71, lutetium. In lanthanide ions, the trivalent lanthanides ( $\text{Ln}^{3+}$ ) are researched for their optical properties. The luminescent properties it shows are due to its unique electronic configuration. In a trivalent lanthanide ion, 5d1 and 6s2 electrons are absent, which gives excited 4f electrons the opportunity to take part in multiple possible radiative transitions directly to the ground state. These radiative transitions give rise to photon emissions, leading to much-desired luminescent properties. Moreover, the partially filled 4f electron shell is shielded by completely filled outer 5s and 5p shells. Due to this shielding, the transitions from the partially filled 4f electron shell are only marginally affected. This is beneficial as the optical transitions occur at almost the same energies for different host lattices. It can be said that the required optical transitions are not much affected by the choice of host lattice[6].

The host material determines the precise nature of the energy level structure, particularly the width and strength of the various transitions, despite the fact that the energetic position of an energy level is mainly unaffected by its surroundings. The host lattice is responsible for the effective broadening of energy levels  $^{2s+1}L_j$  by splitting them into so-called Stark levels (crystal field components). For photovoltaic applications, the effective broadening of energy levels, i.e., a wider absorption spectrum, is highly desirable because it can use a more significant portion of the solar spectrum for upconversion. Recent research includes many fluorides, oxyfluorides, chlorides, oxides and sulfides as possible host lattices.

Organic upconverter materials, on the other hand, offer greater flexibility in terms of design and synthesis. Modifying their molecular structure can be tailored to exhibit specific optical properties. These modifications make them attractive for displays, sensing, and security applications. According to recent research, a few examples of organic upconverters include metal-organic frameworks (MOFs) and covalent organic frameworks (COFs). A few organic upconverters being researched recently are titanyl

phthalocyanine films with tris-(8-hydroxy quinoline) aluminium (Alq3) as an organic light emitting diode OLED and a blend of tin naphthalocyanine (SnNc) with different NIR sensitizer in addition to this thermally activated delayed fluorescence (TADF) emitters are also tested for organic upconverters. These materials have shown promising results in upconversion efficiency and stability.

Additionally, researchers have also explored the use of hybrid materials, such as inorganic-organic composites, to combine the unique properties of both types of materials. One example is using quantum dots as sensitizers for organic upconverters, which has shown improved efficiency and tunability. Other strategies for enhancing upconversion performance include surface modification and doping with rare earth ions. Overall, developing new organic upconversion materials and optimizing existing ones hold great potential for advancing a range of technological applications. Both types of upconverter materials have their own advantages and limitations, and the choice of material depends on the specific application requirements. Our research focuses on rare earth ions' luminescent properties; therefore, in section 1.7, we have discussed a few rare earth ions.

## 1.5 LUMINESCENT LIFETIME

There are various ways excited electrons can get de-excited. Mainly the processes are radiative or non-radiative. The radiative process leads to luminescence, while non-radiative leads to energy loss. Both processes are vital in determining the intensity and lifetime of luminescence observed. A mathematical quantity decay rate constant ( $k$ ) measures the probability of the de-excitation process. It is given by the sum of decay rates of various radiative ( $k_r$ ) and non-radiative ( $k_{nr}$ ) de-excitation processes.

$$k = k_r + k_{nr} \quad (1.1)$$

The reciprocal of the decay rate constant gives the time electrons remain in an excited state.

$$\tau = \frac{1}{k} = \frac{1}{k_r + k_{nr}} \quad (1.2)$$



Therefore, different RE ions amount to different decay rate constants' values. Decay rates for a non-radiative and radiative process differ for each RE ion. The lifetime also contributes to the intensity of luminescence observed. The variation of photoluminescence intensity with time is mathematically expressed as:

$$I_t = I_0 e^{(-t/\tau)} \quad (1.3)$$

Luminescent lifetime ( $\tau$ ) is also defined as the time required by the intensity of luminescence to get reduced to 1/e of its initial value.

## 1.6 RARE EARTH IONS

### 1.6.1 ERBIUM

The chemical element erbium has the atomic number 68 and the symbol Er. Erbium, a solid silvery-white metal when isolated artificially, is always present in chemical combinations with other elements. The metal erbium is pure, soft and silvery. It has a hexagonal lattice structure as a pure solid or a three-dimensional arrangement of atoms. Heat and electricity are both poorly and moderately conducted by erbium. Insulators are another name for poor conductors. It can be burned to make oxides and gradually tarnishes in the air. It forms hydroxides when it reacts slowly with cold water and fast with hot water. In weak acids, it can dissolve to produce erbium ion solutions. Erbium salts are typically pink in colour. In its 6s shell, erbium contains two valence electrons. Erbium often exists in the +3 oxidation state. Erbium, according to recent studies, may aid in boosting metabolism. The element's biological purpose, if any, is still unknown. While the compounds often aren't poisonous to people, the pure metal is marginally hazardous. Bones contain the majority of erbium in the human body. The nuclear industry uses erbium as a neutron absorber. To make other metals easier to deal with and less hard, erbium can be added. For instance, it is frequently added to vanadium to soften it. Pink colourant erbium oxide is utilized in glass and porcelain glazing. The pink colour is also added to cubic zirconia using this technique.  $\text{Er}^{3+}$ , the pink ion utilized in glass and porcelain, is fluorescent and glows in natural and artificial light. Lasers (like dental lasers) and optical fibres can benefit from erbium's intriguing optical characteristics. Erbium has distinct absorption spectra bands in the near-infrared, visible, and ultraviolet light, like related rare earths. Erbium has a significant amount of electrons, which makes it simple

for chemical reactions to remove them. The ionization energy is the amount of energy necessary to eliminate a single electron. Because they have a large number of inner shell electrons that prevent the valence electrons from being drawn to the positively charged nucleus, the lanthanides, including erbium, have some of the lowest ionization energies. Erbium-doped materials have emerged as a central area of research due to their potential use as a dopant. Its wide PL emission range from visible to mid-infrared regions make this a suitable activator. Eye-safe MIR applications in medical technology, remote sensing, air pollution monitoring, and military countermeasures are all possible with erbium-based solid-state lasers.

Furthermore,  $\text{Er}^{3+}$  ions are the most popular luminous dopant for temperature sensing because they have two unique thermally connected energy levels with a tiny energy gap,  $2\text{H}_{11/2}$  and  $4\text{S}_{3/2}$ . Due to its higher energy level structure, triply ionized erbium ( $\text{Er}^{3+}$ ) has proven to be the most effective RE ion for light upconversion effects. However, when stimulated at 980 nm, the  $4\text{I}_{11/2}$  level's narrow absorption cross-section lessens its luminescence potency. In addition to solid photoluminescence, Er-doped-based ceramics have good photochromism, high sensitivity, and a non-destructive reading capacity. The samples exhibit excellent reversibility when alternating thermal stimulation and visible light irradiation. Although erbium does not play a part in biology, its salts can increase metabolism. The typical annual human erbium intake is 1 milligram. Humans have the largest erbium concentration in their bones, which is also present in their kidneys and liver. If consumed, erbium is only mildly poisonous, although its components are not harmful. Erbium metallic in dust form is a fire and explosion risk.

### 1.6.2. SAMARIUM

Samarium is a rare earth element that resembles zinc in terms of hardness and density. Samarium is the third most volatile lanthanide after ytterbium and europium and is equivalent to lead and barium in this regard, with a boiling point of 1,794 °C (3,261 °F). This facilitates the separation of the samarium from its ores. When freshly made, Samarium has a silvery shine, and when it oxidizes in air, it seems duller. With a radius of 238 pm, samarium is thought to have one of the largest atomic radii of all the elements. Freshly processed samarium has a silvery appearance. It slowly oxidizes in the air at room temperature and spontaneously ignites around 150 °C (302 °F). Even when placed

underneath mineral oil, samarium slowly oxidizes and develops a greyish-yellow powder of the oxide-hydroxide mixture near the surface. The metallic appearance of a sample can be preserved by encasing it in an inert gas, such as argon.

Samarium has a rhombohedral structure (shape) in natural settings. Its crystal structure transforms to hexagonal close-packed (hcp) at 731 °C (1,348 °F), with the precise transition temperature depending on metal purity. The metal becomes a body-centred cubic (bcc) phase after additional heating to 922 °C (1,692 °F). A double-hexagonally close-packed structure, or  $d_{hcp}$ , is produced by heating to 300 °C (572°F) and compressing to 40 kbar. A series of phase transitions are brought on by pressures of hundreds or thousands of kilobars, in particular, the appearance of a tetragonal phase at about 900 kbar. The sesquioxide  $Sm_2O_3$  is the most durable samarium oxide. There are various crystalline phases of it, just like many samarium compounds. The slow cooling of the melt produces the trigonal shape.  $Sm_2O_3$  has a high melting point (2345 °C). Hence induction heating using a radio-frequency coil is typically used to melt it instead of direct heating. Trivalent sulphides, selenide, and telluride are the products of samarium. The cubic rock-salt crystal structures of the divalent chalcogenides  $SmS$ ,  $SmSe$ , and  $SmTe$  are known. When pressure is applied to these chalcogenides, they transition from semiconducting to metallic at room temperature. The scientific world has taken notice of  $Sm$  because  $Sm^{3+}$  is a magnetically active amphoteric RE dopant with an ionic radius of 1.24, which is between  $Ba^{2+}$  and  $Ti^{4+}$ .  $Sm_2O_3$  was chosen as a dopant because of its distinctive optical characteristics, which may allow for the formation of extra absorption bands in ceramic structures, a change in electron density, and an increase in the crystallinity level of ceramics. The importance of this research rests not only in addressing the fundamental problem of determining how titanates' structural properties change as a result of doping but also in broadening the scope of their valuable applications.

### 1.6.3 YETTERBIUM

Yb a delicate silver metal. It progressively oxidizes in the air, creating a surface layer of protection. Ytterbium is starting to be used in several applications, including memory systems and tunable lasers. It is increasingly being utilized to replace other catalysts thought to be too hazardous and harmful to replace industrial catalysts. The biological function of ytterbium is unknown. It is not harmful at all. Like many other lanthanide

elements, Ytterbium is primarily found in the mineral monazite. Ion exchange and solvent extraction are two methods for extracting it. Ytterbium ( $\text{Yb}^{3+}$ ) ion-doped laser ceramics have been regarded as some of the most desirable solid-state laser materials among other laser ceramic varieties. High quantum efficiency, a long lifetime of fluorescence, and a broad emission spectrum are just a few of the unique characteristics of the  $\text{Yb}^{3+}$  ion. Direct laser diode pumping benefits greatly from ytterbium's wide absorption band. Due to its high hardness, high thermal conductivity, and stable chemical properties, yttrium aluminium garnet (YAG) is a reasonably common laser host material. To obtain great optical transparency, having a cubic crystal structure is crucial. Ytterbium (III) is similar to the  $\text{Ce}^{3+}$  ion and has a  $f13$  structure. Two electronic levels make up the straightforward energy level system for trivalent ytterbium ions with the electron configuration  $4f13$ . The crystal field is separated into three Stark components for the higher  $2F_{5/2}$  and lower  $2F_{7/2}$  levels. The laser oscillation is due to optical transitions from the lowest  $2F_{5/2}$  stark sub-level to the highest  $2F_{7/2}$  sub-levels. However, ytterbium-doped  $\text{Y}_2\text{O}_3$  ceramics have significantly more spectral bands than are allowed for the optical transition bands in this system.  $\text{Yb: Y}_2\text{O}_3$  ceramics have additional absorbance and luminescence bands, like ceramics and single crystals of yttrium-doped yttrium aluminium garnet ( $\text{Yb: YAG}$ ). The emission and absorption maxima of the penultimate rare earth,  $\text{Yb}^{3+}$ , are in the infrared. It has a straightforward technique for determining energy levels.[7]

The ground state of ytterbium is  $2F_{7/2}$ . Approximately equivalent to  $7/2 \zeta_{4f/2}$  is the distance between the two states  $2F_{5/2}$  and  $2F_{7/2}$ , where  $\zeta$  is the spin-orbit coupling constant, which has a value of  $2924 \text{ cm}^{-1}$ . At  $9700$ , the transition  $2F_{7/2} \rightarrow 2F_{5/2}$  takes place. The two manifolds,  $2F_{5/2}$  and  $2F_{7/2}$ , are divided into three and four sublevels, respectively, with energies that depend on the Stark's effect strength, which is in turn influenced by the host characteristics, the activator typology, and the doping level. Ytterbium-doped media give rise to a quasi-three-level laser system with a broad absorption band ideal for laser-diode pumping and broad emission bands because of this very straightforward energy level scheme. The  $\text{Yb}$  ion can exhibit a relatively tiny quantum defect (10%) due to the proximity of the two mentioned bands, which helps to lower the thermal burden. Furthermore, the sesquioxide (and other hosts) can be heavily doped without significantly distorting the host lattice thanks to  $\text{Yb}^{3+}$ 's modest diameter comparable to that of  $\text{Lu}^{3+}$ ,  $\text{Sc}^{3+}$ , and  $\text{Y}^{3+}$ .

## 1.7 HOST SELECTION

In most cases, the host materials are oxides, nitrides and oxynitrides, sulphides, selenides, halides, or silicates of zinc, cadmium, manganese, aluminium, silicon, or various rare-earth metals. The two types of lead-free piezoelectric materials are inorganic and organic. Most researchers focus on typical inorganic ceramics, such as ZnO nanostructures and ceramic systems based on barium titanate (BT), sodium potassium niobate (KNN), and sodium bismuth titanate (BNT), as well as ferroelectrics with bismuth layer structures[8]. The introduction of PVDF, its copolymers, their composites, and some biopolymers pertains to organic lead-free piezoelectric materials. The first documented lead-free piezoelectric ceramic is a BT-based system with an  $ABO_3$  perovskite structure. Low  $T_c$  and  $d_{33}$  limit the BT-based ceramic system but benefit from steady electrical characteristics, strong electromechanical coupling, and low dielectric loss at room temperature. Improved piezoelectric characteristics have been attained by creating new structures or streamlining the preparation process.

The primary organic lead-free piezoelectric materials, commonly referred to as piezoelectric polymers, are PVDF and other organic piezoelectric materials like epoxy, nylon, and silicone. Recent years have seen a noteworthy increase in the attention of researchers in PVDF, its copolymers, and their composites due to their benefits of low density, substantial flexibility, low impedance, and high piezoelectric constant. Due to these benefits, they are frequently used in creating electroacoustic transducers, ultrasonic transducers, ceramic filters, infrared detectors, and other devices.

In this dissertation thesis, the focus has been driven to inorganic host materials, mainly KNN.

## CHAPTER 2

### LITERATURE REVIEW

#### 2.1 LEAD-FREE KNN CERAMIC

In the realm of electromechanical conversion, potassium sodium niobate (KNN), a piezoelectric ceramic material, offers a possible substitute for lead-based piezo ceramics. Near morphotropic phase boundary regions, KNN ceramics exhibit superior electrical characteristics[9]. One of the most promising, environmentally acceptable, lead-free candidates to replace highly effective, lead-based piezoelectrics is potassium sodium niobate or  $K_{0.5}Na_{0.5}NbO_3$ . Because KNN is famously challenging to sinter and densify, processing conditions must be taken into account. The hysteresis behaviour in relation to sintering temperature has been studied [31]. The researchers demonstrated that a sintering temperature of 1020°C resulted in a theoretical density of 69.4%, and they found no evidence of hysteresis behaviour, which may have been caused by insufficient densification. The identical formulation yielded fully saturated hysteresis loops when sintered at 1080°C when densification reached a substantially higher theoretical density of 94.4%, demonstrating how crucial the sintering temperature is when processing NKN ceramics. Since the early KNN studies, it has been acknowledged that generating phase-pure materials with a high density and a consistent, fine-grained microstructure is extremely difficult[10]–[12]. This is why the current research examines the various techniques for consolidating KNN ceramics. The main concern of developing research is the challenges of attaining phase purity, the stoichiometry of the perovskite phase, and chemical homogeneity in the solid-state production of KNN powder. Stoichiometric KNN's solid-state sintering is characterized by inadequate densification and a petite temperature range that is near the solidus temperature. According to research on the first sintering stage, microstructure coarsening without densification lowers the driving force for sintering. Discussion is held regarding the effects of the (K+Na)/Nb molar ratio, the existence of a liquid phase, chemical alterations (doping, complicated solid solutions), and various atmospheric conditions (i.e., defect chemistry) on the sintering. The density of KNN ceramics can be increased using specialized sintering processes, including

pressure-assisted sintering and spark-plasma sintering. A typical piezoelectric lead zirconate titanate (PZT) is used to compare the sintering behaviour of KNN to that of PZT. The main benefits of KNN over other lead-free compositions include its low density, biocompatibility, high mechanical quality factors[13], fatigue resistance, decent temperature stability of the piezoelectric properties, and, as of late, its compatibility with inexpensive base-metal electrodes[14]–[17]. These materials have not only caught the interest of scientists but also of business, and the prototypes and finished goods have begun to appear: ultrasonic transducers, ultrasonic motors[18], multilayer actuators[19], knock sensors, and piezoelectric transformers[20][21]. Despite their hopeful features, KNN-based piezoelectrics are still not frequently used in industrial applications. Processing-related issues include challenges in generating high densities of sintered products, stoichiometry deviations and the resultant development of secondary phases, and challenges in controlling the microstructure[16], [22]. Such phenomena should be carefully handled since they might cause uneven distributions of the applied electric fields, leakage currents, low breakdown fields, poor repeatability, and poor piezoelectric performance of the ceramics. A-site  $\text{Na}^+$  and  $\text{K}^+$  are lost due to volatilization as the sintering temperature rises, which causes an increase in the number of A-site vacancies in the lattice. When NKN is doped, its usual orthorhombic structure may transform into a tetragonal one. At this point, doping NKN causes the orthorhombic to tetragonal polymorphic phase transition to cool to ambient temperature (from about  $200^\circ\text{C}$ ). There are two primary methods for differentiating the phases due to the similarity of the XRD spectra for these two phases: orthorhombic and tetragonal phase features[21].

## 2.2 SCOPE OF OUR WORK

As indicated before, KNN-based piezoceramics have high  $T_c$  and good piezoelectric performance. Therefore, KNN-based piezoceramics are viewed as potential replacements for their lead-based application equivalents. Several uses, including inkjet printing and multilayer actuators, have been mentioned. In some ways, KNN-based piezoceramics outperform lead-based ones and fit these applications. KNN-based materials can be used in a multilayer actuator due to their excellent compatibility with nickel electrodes made of base metal[19]. Due to their accurate response as a function of the applied voltage and rapid reaction rate, piezoelectric materials are frequently used as the actuating unit. An example of a standard commercial product that uses piezoelectric components is inkjet

printing. The ink chamber will be squeezed when an electric field is provided to the piezoelectric device, and the ink can then be expelled from the valve. The multilayer actuators have also been equipped with KNN-based piezoceramics. For example, the multilayer structure is typically used in fuel injectors, where a significant displacement and a low driving voltage are necessary. KNN-based piezoceramics are also used in multilayer actuators. The piezoelectric strain performance of the multilayer actuators based on KNN is about half that of the actuators based on PZT. However, the issue can be readily resolved by stacking more piezoceramic layers that are thinner than one another[23].

Additionally, when the piezoelectric element squeezes the chamber, KNN-based multilayer actuators incur a penalty. The PZT-based multilayer actuators have the disadvantage of being unable to use base-metal materials as electrodes, such as nickel, while the multilayer actuator that actuates in response to the applied electrical signal can. A piezoelectric energy harvester has an advantage over a conventional battery since it can capture vibrational energy from the surrounding environment and store it using an appropriate electrical circuit design[24]. However, several intriguing studies have been conducted on the novel and possible uses of KNN-based piezoceramics, including those on energy harvesting, structural health monitoring, piezoelectric filtering membrane, and tissue regeneration. Piezoelectric energy harvesters have grown in importance due to the miniaturization of contemporary electronics and their built-in power sources.



## CHAPTER 3

### FABRICATION AND CHARACTERIZATION

#### 3.1 SOLID-STATE REACTION METHOD

Solid-state reactions are those that occur between solids. Classically, it is defined as a reaction in which the product is solid, and both reactants are solid. However, in practice, many reactions are classified as solid-state reactions even though both reactants are not solid. For instance, one of the reactants in the rusting of iron, which is categorized as a solid-state reaction, is solid, and the other is gaseous. Due to the fact that many polycrystalline solids can only be produced by this technique, the study of solid-state reactions has assumed great importance. Solid-solid reactions are not simple and require various conditions for their progression. The structural analyses of the product include a variety of approaches as well[25].

The process of fine-grain metal combinations involves mixing different metal combinations, forming pellets, and subjecting them to controlled temperatures for a specific duration. Some metal compounds, such as metal oxides or salts, require extreme conditions like high temperatures and pressure to initiate reactions in a molten flux or rapidly condensing vapour phase. This technique is commonly referred to as "shake and bake" or "heat and beat" chemistry.

In solid-state synthesis, it is crucial to describe the reaction rate. Solid-state processes must be completed thoroughly as options for purifying produced solids are limited. The reaction rate in solid-state reactions depends on various factors, including the structural properties, shape, and surface area of the reactants, diffusion rate, and thermodynamic factors associated with nucleation and reaction. The chemical precursors and preparation methods employed play a significant role in determining the chemical and physical properties of the final products.

Modern solid-state preparation techniques extend beyond variations of the ceramic process. In solid-state metathesis, the reactions of metal compounds are initiated by an

energy source such as a flame or a ball mill, and the heat generated during product formation and byproduct production promotes these reactions.

### 3.2 SAMPLE PREPARATION

Our research used a solid-state reaction route to synthesize the potassium sodium niobate with the chemical formula ( $K_{0.5}Na_{0.5}NbO_3$ ). Pure and rare earth ion-doped KNN is synthesized. In this research, rare earth ion erbium is used. Chemically rare earth ion is doped according to the weight percentage of pure potassium sodium niobate. Thus, the chemical formula [ $K_{0.5}Na_{0.5}NbO_3: x \text{ wt}\% \text{ Er}^{3+} = 0,1,2,3,4$ ] is abbreviated as KNN:xEr ( $x=0,1,2,3,4$ ).

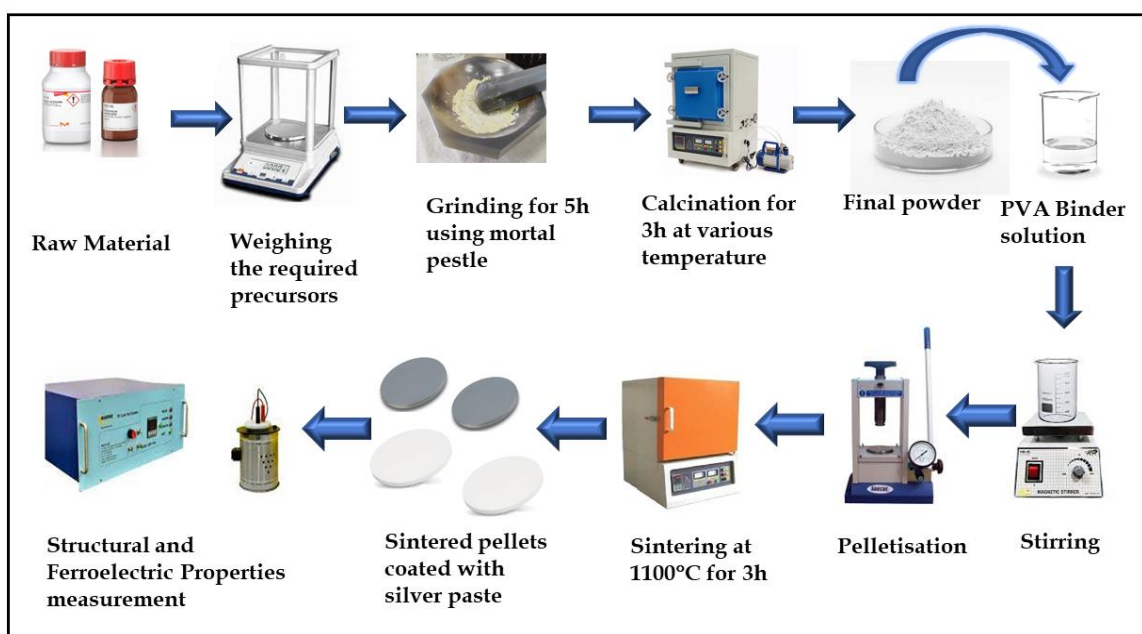


*Figure 3 Schematic Diagram of Synthesis Process*

The precursors used were potassium carbonate, sodium carbonate, niobium oxide and erbium oxide in powder form with 99.99% purity. The powders were grounded in a mortar pestle using ethanol for 5h after mixing in a stoichiometric ratio. The hand-ground powders are calcined for 3h. After calcination, the calcined powders are tested for unreactive residue. The sample with the least amount of residue is mixed with a 5% PVA solution. The PVA is a standard binder it helps in making pellets of powders. After pressing the calcined powder in pellets of 1mm thickness, the pellets are sintered. The sintering temperature is taken to be 1100°C. The pellets are sintered for 2h with 1h sintering at midway temperature 500°C. Keeping the temperature midway obliterates the

binder solution[26]. Similarly, the described process is used to fabricate the whole series of KNN with different erbium ion compositions.

### 3.3 CHARACTERIZATION

#### 3.3.1 STRUCTURAL CHARACTERIZATION- XRD

There are various structural characterization techniques available. Some of the most widely used spectroscopies are X-ray diffraction (XRD), Transmission Electron Microscopy (TEM), Scanned electron microscopy (SEM), and neutron magnetic resonance (NMR) spectroscopy. In lieu of this research, we will only focus on XRD for structural analysis, i.e., the crystallite nature of the synthesized material, which includes the degree of crystallinity, phase identification, lattice characteristics, and grain size.

The X-ray powder diffraction method follows Bragg's law to analyze the crystal's nature. The following expression gives it:

$$2d \sin \theta = n\lambda \quad (3.1)$$

The mechanism of X-ray diffraction is such that the X-ray target the inner electrons of an atom. After interacting with the inner electrons, the scattered X-ray interacts within the vicinity of the atom. The interaction results give detailed information about the periodicity of atom arrangement in the material. The scattered X-rays constructively or destructively interfere with each other. The Bragg's law mathematically expresses constructive interference. The x-ray graph shows high peaks for constructive interference implying high intensity of scattered x-ray. Using the Bragg's law, the interplanar spacing 'd' is calculated for each peak at a particular angle. Each peak observed in the X-ray pattern represents a specific Miller index. Each compound's unique X-ray pattern is available for scientific purposes. The powder diffraction file (PDF) contains x-ray patterns of all the possible compounds. For research motives, the JCPDF file for a specific compound is downloaded, and the X-ray results are matched to confirm the purity of phase formation.

#### 3.3.2 CHEMICAL CHARACTERIZATION- FTIR

FTIR analytical technique identifies the chemical structure of organic and inorganic materials. FTIR analysis is based on the wavelength of infrared radiations absorbed by a

material. And only radiations with specific frequencies are absorbed by a material; it depends on the molecular bonds as different molecular bonds vibrate at different frequencies. In the FTIR spectra, the wavelengths absorbed are indicated as dips. The FTIR spectra of each material are unique, just like DNA or fingerprints. So, its analysis gives us quite detailed information about the different molecular bonds present in the material. FTIR spectroscopy is more beneficial than other infrared spectroscopies as it is faster and more precise and does not harm the sample.

### 3.3.3 OPTICAL CHARACTERIZATION – PL

There are various optical characterization techniques. Optical characterization is used to measure photoluminescence, luminescent lifetime etc. This research analyses visible down-conversion photoluminescence, upconversion luminescence and time-resolved luminescence spectroscopy. Photoluminescence spectroscopy is an optical method to analyze the electronic configuration of a material. Fundamentally, optical characterization uses light to investigate a material's physical and chemical properties. Photoluminescence relies on photoexcitation, in which the material, when irradiated with a laser beam, causes the electrons to get excited and emit photons when relaxing back to the ground state via characteristic radiative and non-radiative phenomena. This excitation spectrum is particular to the energy difference between the ground and the excited states. Hence, beneficial to understand the properties of the material being characterized. Photoluminescence spectroscopy analyzes the phosphorescence and fluorescence, which in turn can be used to study the optoelectronic properties of many semiconductors, ceramics and phosphors.

### 3.3.4 ELECTRIC CHARACTERIZATION

Variables like conductance, resistance, inductance, polarizability, and dielectric constants are analyzed using electric characterization. Electric characterization is crucial to study ferroelectrics, dielectric, and piezoelectric materials. Our research focuses on ferroelectric material, and we will focus on the material's behaviour with varying electric fields. As ferroelectric materials have good hysteresis loops. Our study focuses on the P-E hysteresis loop and its variance. With the P-E loop energy storage capacity of a material is also calculated, which helps determine the potential of a material to be used in optoelectrical devices.

The most crucial measurement in describing the electrical properties of a ferroelectric ceramic is the hysteresis loop, which represents the relationship between polarization and electric field. Despite the absence of a significant amount of ferro or iron, ferroelectric materials derive their name from the resemblance of this loop to the magnetic loop (magnetization versus magnetic field) observed in ferromagnetic materials. By examining the hysteresis loop, valuable insights into the switching behaviour of the ferroelectric material can be obtained. Furthermore, important parameters, including coercive field, remnant polarization, and saturation polarization, can be determined. This information plays a vital role in the design and optimization of various ferroelectric devices such as capacitors, actuators, and sensors.

## CHAPTER 4

### EXPERIMENTAL RESULTS

#### 4.1 X-RAY DIFFRACTION

The fig. 4(a-e) illustrates the X-ray diffraction (XRD) pattern of pure KNN (potassium sodium niobate) that underwent calcination at different temperatures ranging from 700°C to 900°C. As the calcination temperature increased, there was a noticeable reduction in the intensity of small peaks, indicated by the symbol "\*", suggesting the formation of a more uniform and single-phase structure. However, it cannot be definitively concluded that the structure became completely single-phased after calcination since some small peaks still remained, indicating the presence of minor impurities. Nonetheless, these slight impurities did not have a significant impact on the overall X-ray diffraction pattern.

As the calcination temperature gradually increased from 700°C to 900°C, there was a clear increase in the intensity of X-ray reflections from various crystal planes. At 900°C, a strong reflection arising from the [020] plane was observed, indicating the presence of a well-defined unit cell structure in the crystal of the KNN sample. The occurrence of peak splitting near 46° and broadening in the diffraction patterns implies that the structure exhibits an orthorhombic perovskite arrangement[27]. Specifically, the splitting of the (022) and (200) peaks around 46°, with the (022) peak having a higher intensity, confirms the presence of an orthorhombic lattice[28], [29]. The XRD analysis also revealed the existence of all expected reflections corresponding to the  $Amm2$  space group, matching the reference number 98-024-7571 in the inorganic crystal structure database (ICSD), which denotes an orthorhombic crystalline arrangement[30].

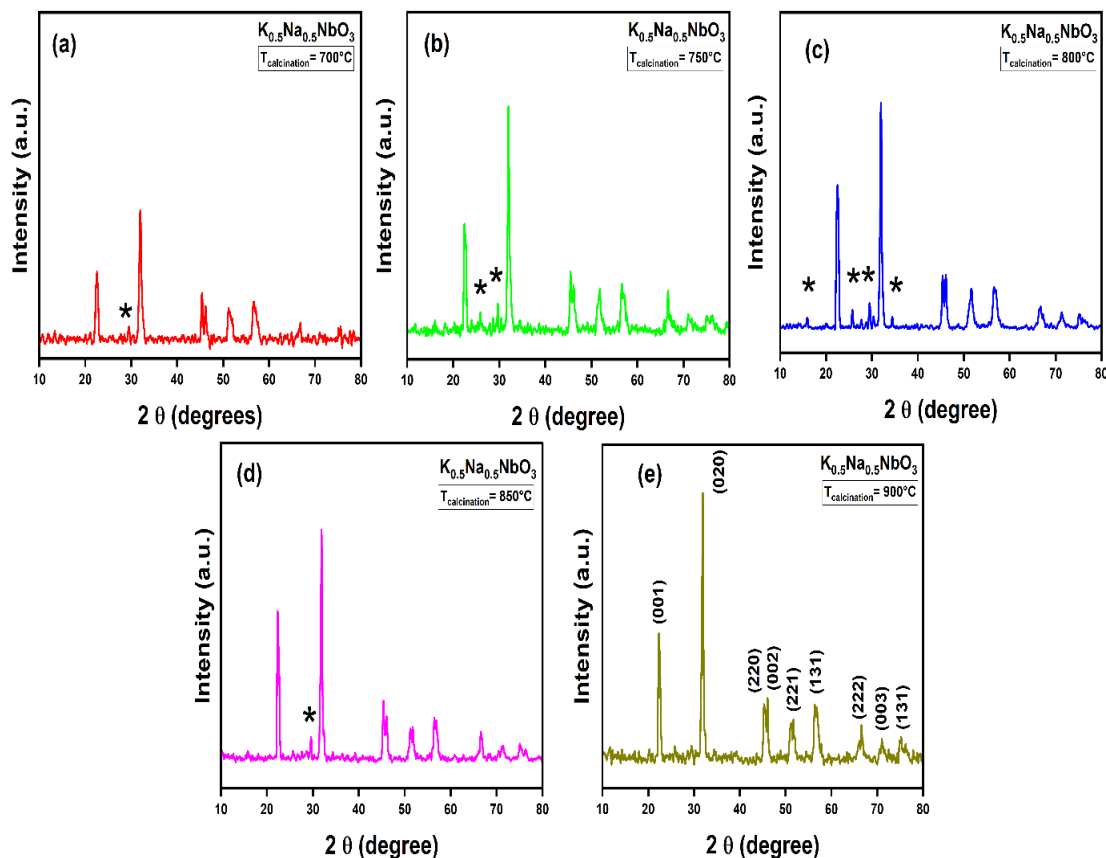


Figure 4(a-e) XRD spectra of pure KNN ceramic calcined at different temperatures ( $T=700^{\circ}\text{C}$  to  $900^{\circ}\text{C}$ )

Fig. 5(a) illustrates the X-ray diffraction (XRD) pattern of KNN: xEr ceramics with different concentrations of Er<sup>3+</sup> ions that were sintered at 1100°C. The presence of the perovskite structure is observed in all the ceramics, indicating the successful diffusion of Er<sup>3+</sup> ions into the KNN host lattice.

In Fig. 5(b), it can be seen that the intense peak corresponding to the (020) plane shifts towards higher angles as a result of the incorporation of Er<sup>3+</sup> ions. This shift in the peak position is attributed to the presence of Er<sup>3+</sup> ions, which have a smaller ionic radius of 1.25 Å compared to the A-site cations (K and Na). The ionic radii for K<sup>+</sup> and Na<sup>+</sup> are 1.64 Å and 1.39 Å, respectively. Due to the smaller size of Er<sup>3+</sup> ions, they occupy the A sites (K and Na), leading to a decrease in the interplanar spacing ( $d$ ). Consequently, the XRD peak corresponding to the (020) plane shifts towards higher angles, resulting in peak shifting.

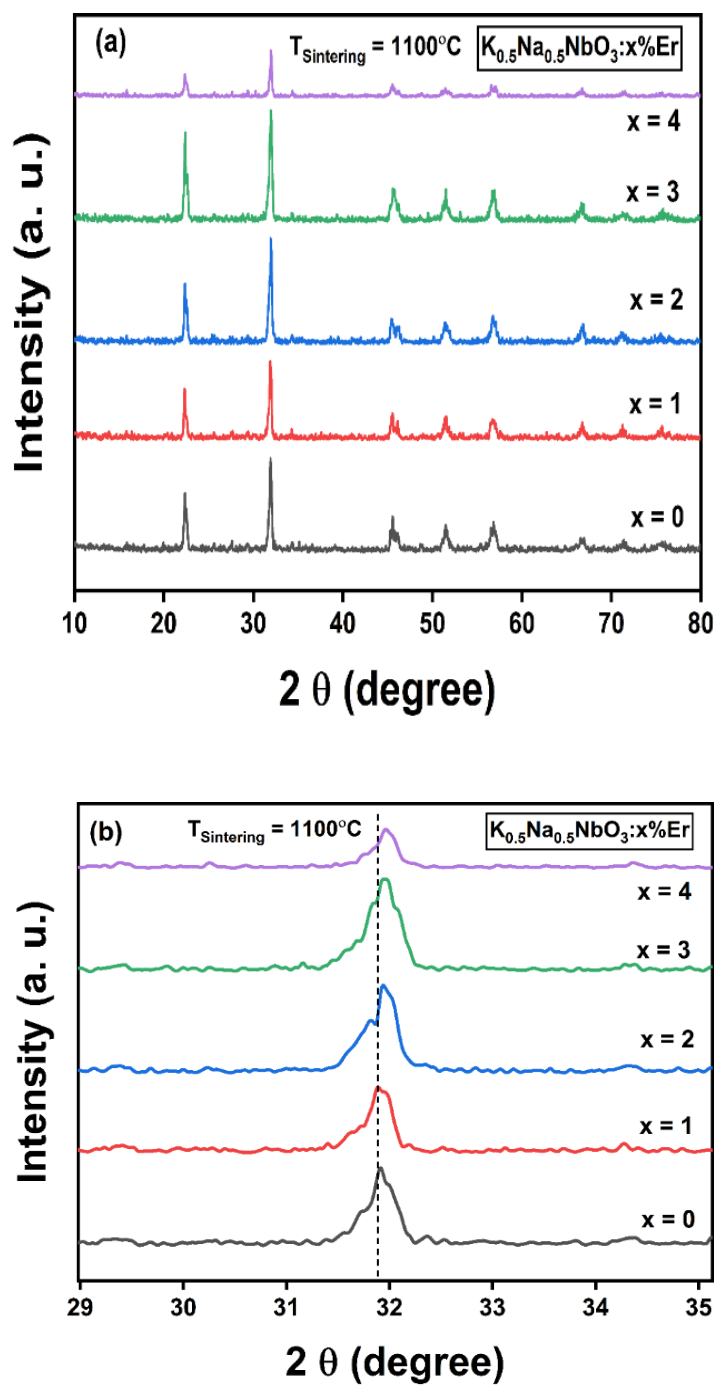


Figure 5(a) Xrd Spectra of  $KNN:xEr$  ( $x=0,1,2,3,4$ ) sintered at  $1100^\circ\text{C}$  (b) XRD spectra displaying peak shifting

#### 4.2 VISIBLE DOWNCONVERSION PHOTOLUMINESCENCE (PL)



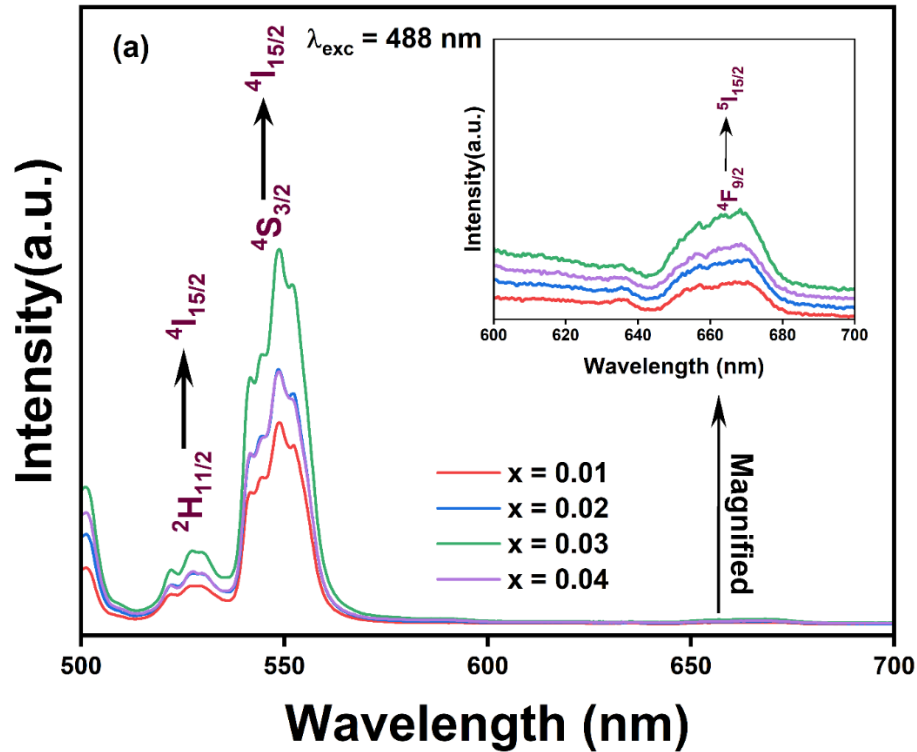


Figure 6 Visible Down Conversion Photoluminescence of KNN:xEr  $x=1,2,3,4$

The fig. 6 exhibits audible down conversion photoluminescence, with the major green emission occurring near 528 nm and 549 nm, respectively, due to the transitions  $2H_{11/2} \rightarrow 4S_{3/2}$  and  $2H_{11/2} \rightarrow 4I_{15/2}$ . The transition  $4F_{9/2} \rightarrow 4I_{15/2}$  is responsible for the very weak red colour radiation at 662 nm [31], [32]. The electrons are directly excited to the  $2H_{11/2}$  and  $4S_{3/2}$  levels upon excitation by a wavelength of 488 nm, which explains for the substantial intensity of both green and red colour emissions via down-conversion. These levels encounter both radiative and non-radiative emissions at the same time. When energized by the light source at 488 nm,  $Er^{3+}$  ions are stimulated to the  $4F_{7/2}$  level. Due to the maximum MPR rate, the majority of stimulated  $Er^{3+}$  ions first reach the  $4S_{3/2}$  level through non-radiative relaxation, and subsequently they reach the  $4I_{15/2}$  ground level through radiation relaxation [33]. This shows that the green fluorescence observed in the KNN is caused by  $Er^{3+}$  and not by any other particles in the lattice.

#### 4.3 UPCONVERSION LUMINESCENCE (UCL)

The observed emission bands in the UC spectrum align with previous research conducted on different hosts that were doped with  $Er^{3+}$  ions [34]–[37]. In Figure 7(a), the luminescence spectrum of KNN: xEr is presented, utilizing a diode laser lamp as the 980

nm wavelength source. Within the spectrum, two distinct fluorescence peaks of green colour are prominently visible at 528 nm and 549 nm, along with a less pronounced red band at 662 nm. The presence of the red colour can be attributed to the 4f-4f transition occurring within the  $\text{Er}^{3+}$  ions (as shown in the inset of Fig. 7(a)). The primary peaks observed at 528 nm and 549 nm in the luminescence spectrum correspond to the energy levels  $2\text{H}_{11/2}$  and  $4\text{S}_{3/2}$  of  $\text{Er}^{3+}$  ions, respectively. These energy level transitions result in the emission of photons as  $\text{Er}^{3+}$  ions transition to the ground state  $4\text{I}_{15/2}$ . Additionally, a weaker fluorescence peak at 662 nm is observed, which corresponds to the transition from the energy level  $4\text{F}_{9/2}$  of  $\text{Er}^{3+}$  to the ground state  $4\text{I}_{15/2}$ .

The intensity of up-conversion luminescence (UCL) increases with higher concentrations of  $\text{Er}^{3+}$  ions. However, at a certain point, typically at  $x = 3$ , the UCL intensity reaches its maximum level. Beyond this concentration, the UCL intensity decreases as more  $\text{Er}^{3+}$  ions are inserted into the host lattice. This decrease is attributed to the concentration-quenching effect, where high concentrations of  $\text{Er}^{3+}$  ions interact and hinder the efficient emission of photons.

Fig. 7(b) depicts the relationship between up-conversion luminescence (UCL) intensity and varying concentrations of  $\text{Er}^{3+}$ . As the concentration of the dopant reaches a critical threshold, the distance between erbium ions becomes extremely small, facilitating easier energy transfer and contributing to non-radiative relaxation. This results in a reduction in radiative transitions and subsequently diminishes the strength of the photoluminescent (PL) emissions[24].

However, when excited at a wavelength of 488 nm, the red and green emissions are relatively weak compared to excitation at 980 nm. Excitation at 488 nm directly excites the electrons to the  $4\text{F}_{7/2}$  energy level. The subsequent multi-phonon relaxation of the  $4\text{F}_{7/2}$  energy level leads to non-radiative processes, simultaneously occupying the mixed energy levels of  $2\text{H}_{11/2}$  and  $4\text{S}_{3/2}$ . Only a limited number of electrons are able to reach the  $4\text{F}_{9/2}$  energy level, from which they transition radiatively to the ground state  $4\text{I}_{15/2}$ , emitting photons in the green and red colours with wavelengths of 549 nm and 662 nm, respectively. This demonstrates that the up-conversion transitions differ significantly between excitation at 980 nm and 488 nm[38].

As illustrated in Figure 7(c), under 980 nm excitation, a larger number of  $\text{Er}^{3+}$  ions are excited to the transitional level, resulting in an increased population of the  $4\text{F}_{9/2}$  energy level through energy transfer (ET). This type of energy transfer is not achievable when stimulated at 488 nm.

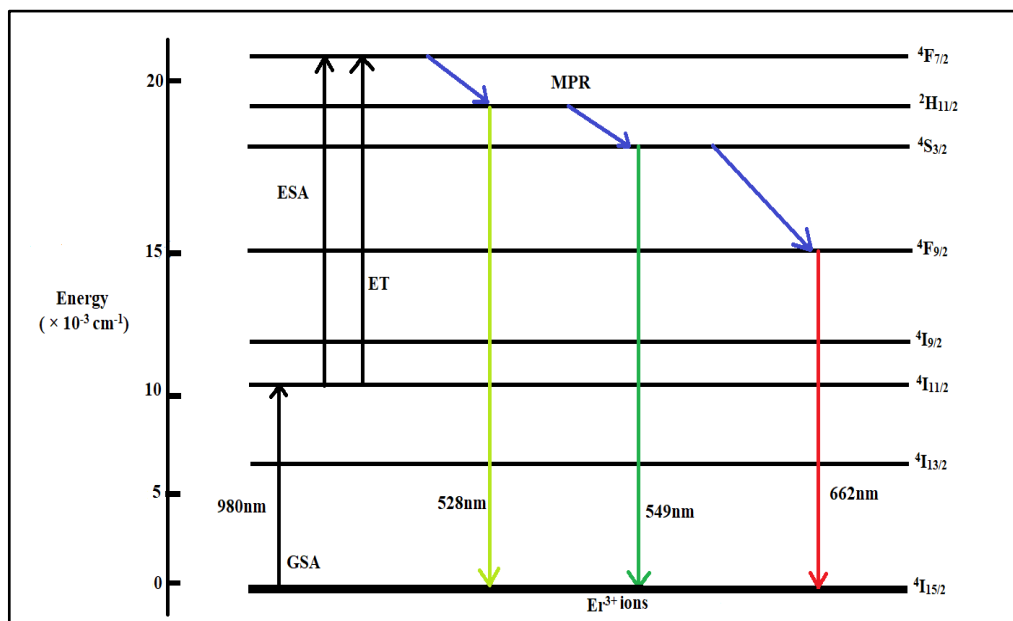
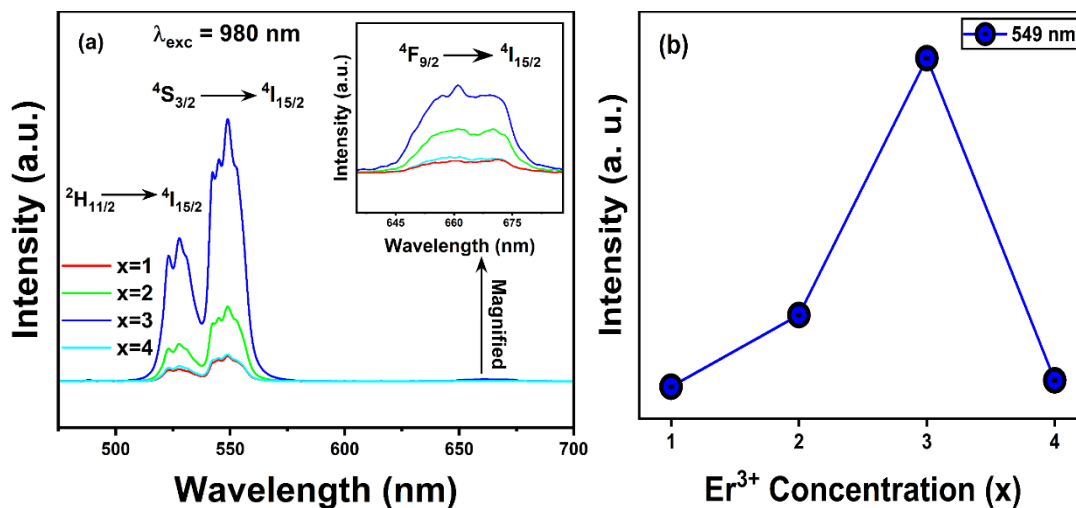


Figure 7 a) Plot of Upconversion luminescence using source wavelength 980nm of KNN: $x\text{Er}$  ( $x=1,2,3,4$ ) b) Plot of intensity vs erbium ion concentration c) Energy level diagram of Erbium.

#### 4.4 INFLUENCE OF PUMP POWER ON UCL

In Fig. 8(a-d), the connection between the overall intensity (I) of each emission band and pumping power (P) has been displayed. For all Er<sup>3+</sup> concentrations, the UCL intensity rises as pump power rises.

Theoretical examination of the multi-photon absorption process suggests a power law mathematical expression between the intensity I and pump power P, as shown in eq. (4.1) [39]–[41]:

$$I \propto P^n \quad (4.1)$$

where n is the number of photons required to complete the UCL mechanism. Three straight lines with positive slopes (denoted by n) for each dopant concentration have been calculated for all emission bands in the log-log plot displayed in Fig. 10(a-d). A log-log scale can be used to plot emission intensity versus excitation power and estimate the properties of the upconversion phenomena, or the quantity of photons absorbed during the upconversion phenomenon. By linearly fitting the experimental data to an equivalent of 2, the slope (n) for the emission bands roughly at 528, 549, and 662 nm is determined. This demonstrates that two pump photons, specifically the red and green UC emissions, took part in each transformation[42].

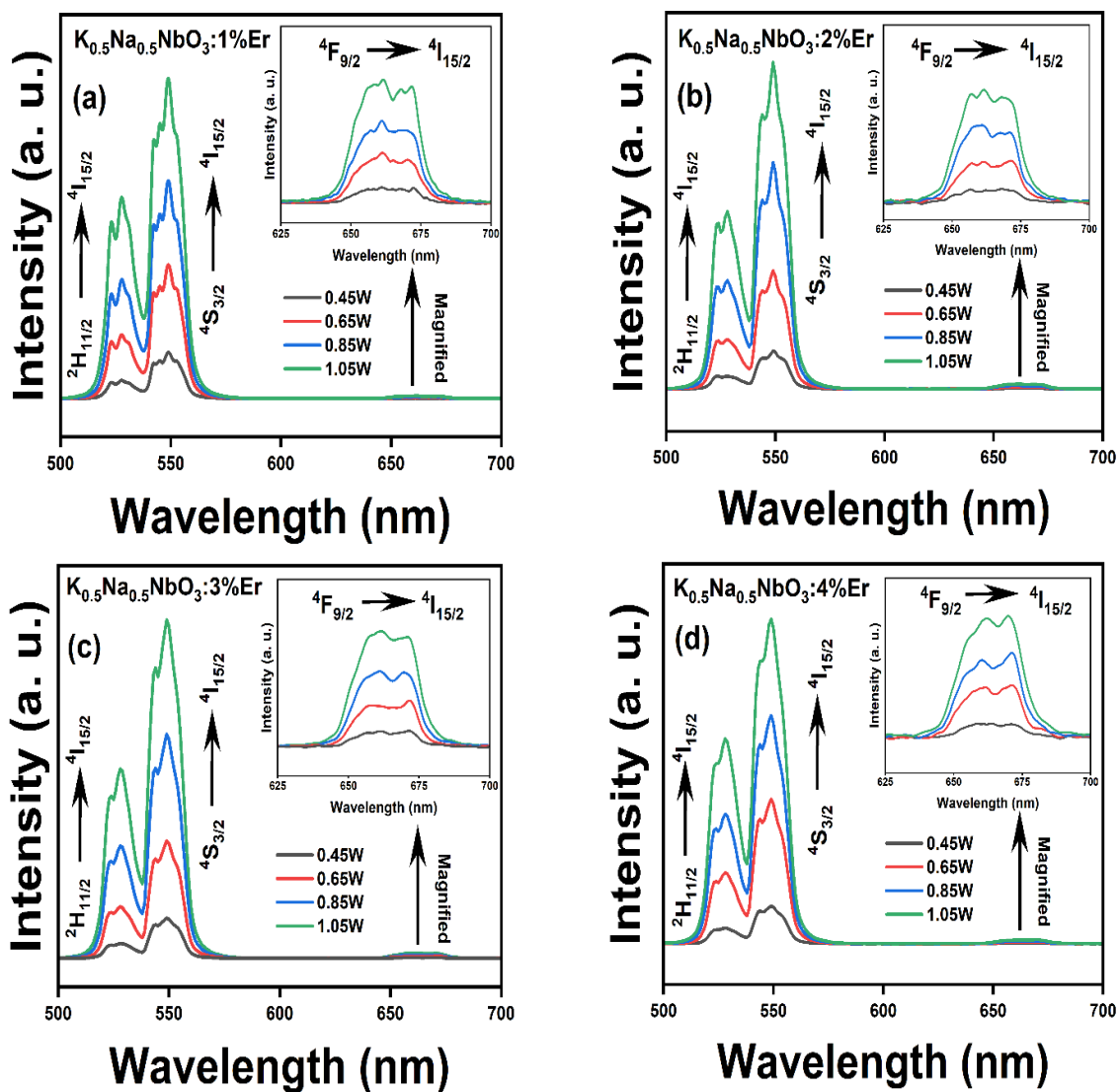


Figure 8 The emission spectra of upconversion (UC) with increasing pumping power for different concentrations of dopants.

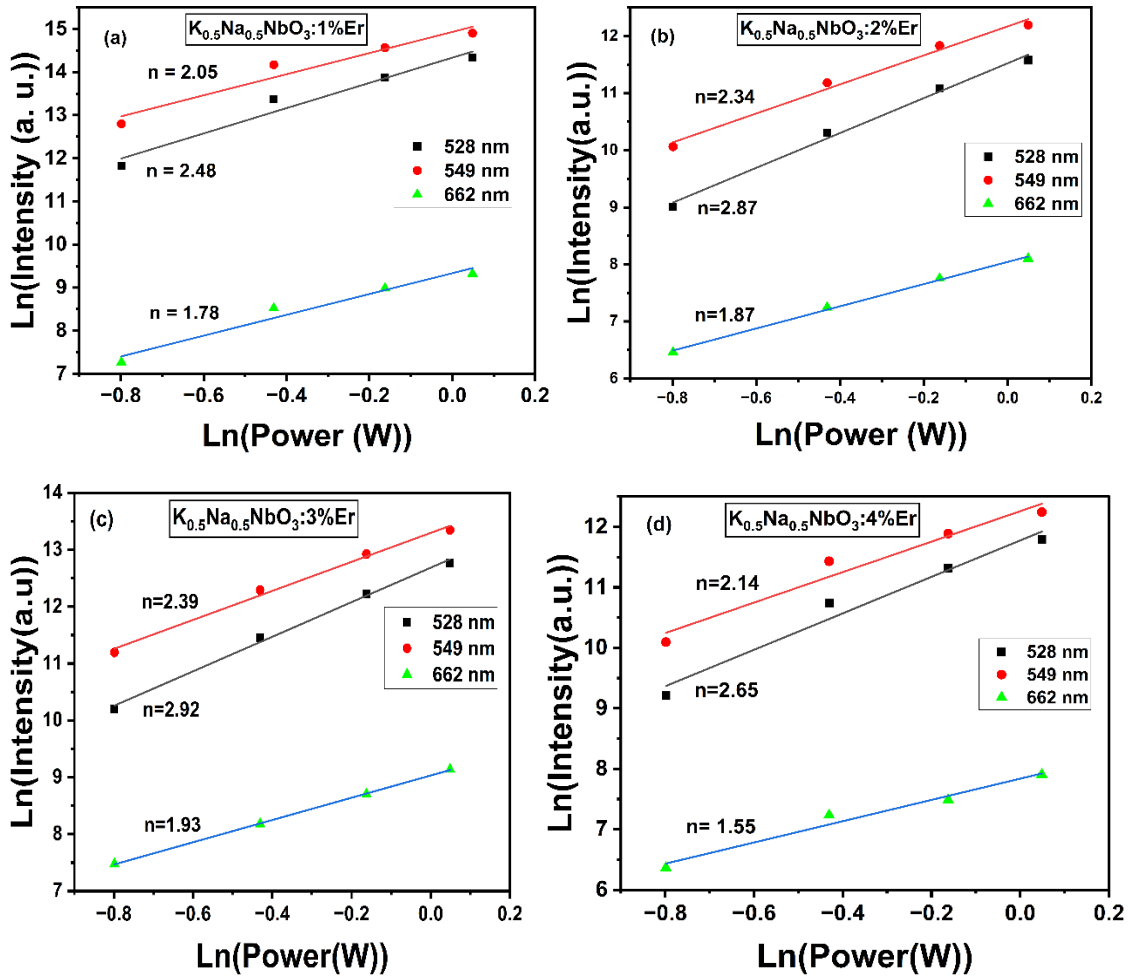


Figure 9 Log-log plot of KNN:xEr (x=1,2,3,4) ceramic.

#### 4.5 TIME DECAY ANALYSIS

When Er<sup>3+</sup> ions were activated with a laser at 980 nm, their emission at 549 nm was observed in the time-resolved photoluminescence (TRPL) decay curve. The temporal decay profile for the 4S<sub>3/2</sub> → 4I<sub>15/2</sub> level at room temperature is shown in Fig. 10. With a tri-exponential decay function for Er<sup>3+</sup> as indicated by given equation, it was sufficient to fit the decay patterns of singularly doped systems.

$$I(t) = A_0 + A_1 e^{-t/\tau_1} + A_2 e^{-t/\tau_2} + A_3 e^{-t/\tau_3} \quad (4.2)$$

Here, I(t) denote the variation in luminous intensity over time, A<sub>i</sub> denotes the scalar quantities, t denotes the measurement time, and i is the decay period at which the population of the excited state drops to 1/e of its starting value. The average lifespan is

calculated using the generalized equation for tri-exponential fit with  $i = 1, 2,$  and  $3$  [43]. It was determined that the average time was  $25.05 \mu\text{s}$  after all the values in the below equation were substituted.

$$\tau_{\text{avg}} = \frac{\sum A_i \tau_i^2}{\sum A_i \tau_i} \quad (4.3)$$

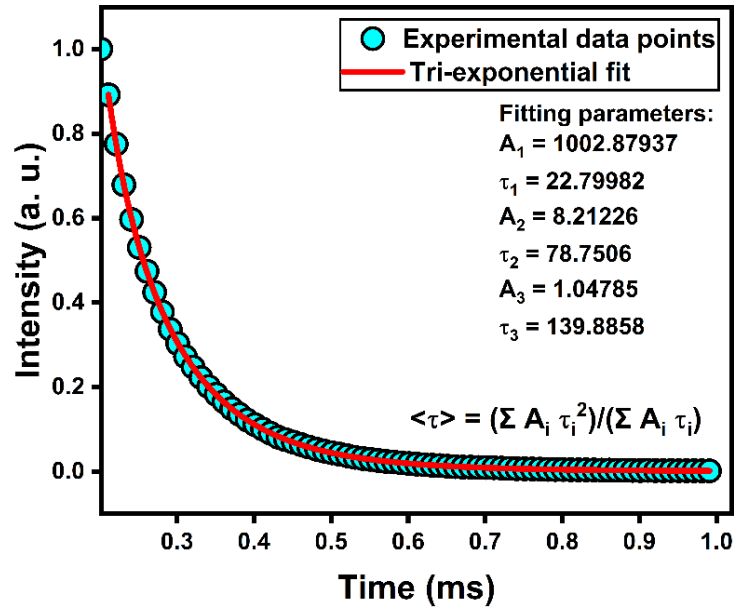


Figure 10 Time decay curve of KNN:xEr ceramic

#### 4.6 FOURIER TRANSFORM INFRARED SPECTROSCOPY (FTIR)

KNN ceramics were sintered at  $1100^\circ\text{C}$  temperatures and then underwent FTIR examinations to discover more about their chemical connections and functional groups. Fig. 4(a) shows the FTIR spectra for KNN: xEr ( $x = 0, 1, 2, 3,$  and  $4$ ) that were obtained. The stretching and bending of the  $\text{NbO}_6$  correspond is responsible for the high-intensity transmittance band at  $486 \text{ cm}^{-1}$  [24]. And the oxygen octahedral, the KNN-specific peak, is responsible for the less dominant band at  $720 \text{ cm}^{-1}$  [44]. The peak shift in Fig. 4(b) from  $471 \text{ cm}^{-1}$  to  $486 \text{ cm}^{-1}$  indicates that the introduction of a foreign ion makes the FTIR spectra more prone to changes in the local structure of the material[45].

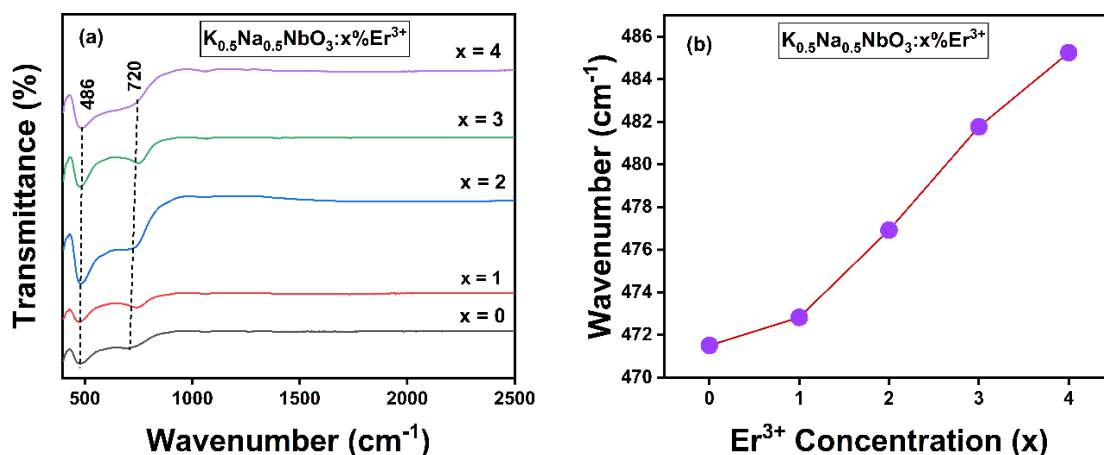


Figure 11 a) FTIR spectra of KNN ceramic with varying  $\text{Er}^{3+}$  weight percentage. (b) Variation of FTIR mode with erbium content.

## 4.7 FERROELECTRIC PROPERTIES

### 4.7.1 PE LOOP ANALYSIS

Fig 12 gives the P-E loop observed for KNN:xEr ( $\text{x}=0,3$ ) and table gives the measured values of remanent and coercive fields. Both samples exhibit hysteresis loops that are in good shape, which is evidence that KNN is a good ferroelectric. When the applied electric field is increased up to 31 kV/cm, the remnant polarisation and coercive field both increase to a maximum of 5.1 C/cm<sup>2</sup> and 8.5 kV/cm, respectively, for the undoped KNN, which is denoted by the notation ( $\text{x} = 0$ ). When the voltage was higher than 31 kV/cm, the undoped KNN was unable to acquire the desired shape, which led to the formation of lossy loops. The electric field higher than 31kV/cm (31 kV/cm to 37 kV/cm) do not cause the hysteresis loop for doped KNN: xEr ( $\text{x} = 3$ ) to lose its form. Both the remnant polarisation and the coercive field drop to 3.17 C/cm<sup>2</sup> and 6.24 kV/cm, respectively, as the field strength decreases. There is relaxation in structural distortion as indicated by the diminishing remnant polarisation. This has also been connected to the structural distortion observed through XRD and FTIR. It is possible for the loss of K/Na to form oxygen vacancies, and it has been found that, in the presence of high electric fields, these vacancies migrate to regions of low energy at domain walls and electrode interfaces. Because of this, polarisation switching can be hindered as a result of domain pinning, which also increases the coercive field [46].



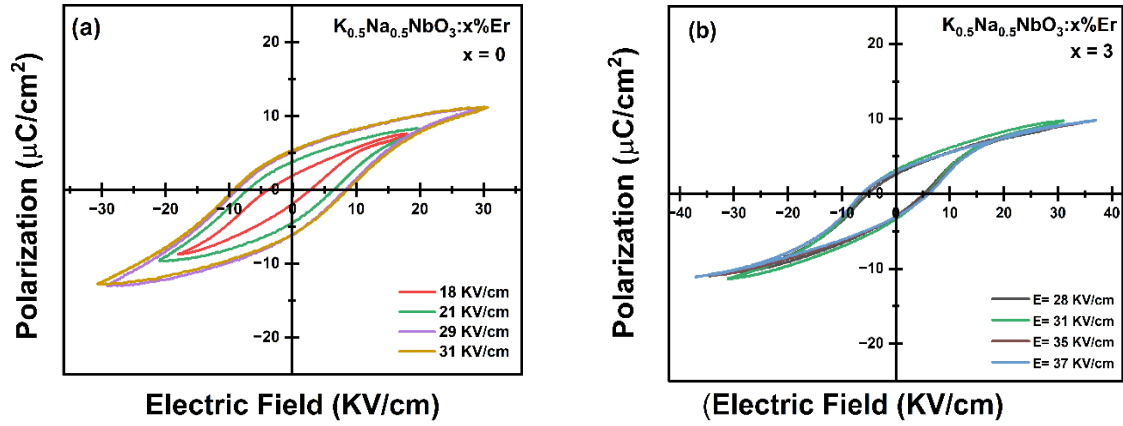


Figure 12 Hysteresis loop of KNN ceramic a) Pure KNN with zero erbium doping b) KNN with  $x=3\text{wt}\%$  Er

Table:1 PE dynamics of KNN: xEr ( $x = 0$  and 3) for various electric fields.

Er <sup>3+</sup> concentration	Electric Field, E (kV/cm)	Remnant Polarization, 2P <sub>r</sub> (μC/cm <sup>2</sup> )	Coercive Field, 2E <sub>c</sub> (kV/cm)
x = 0	18	3.702	5.462
	21	7.592	13.474
	29	10.202	17.124
x = 3	28	5.192	10.384
	31	6.356	11.364
	35	5.788	11.798
	37	6.058	12.478

#### 4.7.2 ENERGY STORAGE CAPACITY

$$W = \int_0^{P_m} E dP \quad (8)$$

$$W_d = \int_{P_r}^{P_m} E dP \quad (9)$$

$$\eta = \frac{W_d}{W} \times 100\% \quad (10)$$

The energy storage characteristics are given by few parameters namely; energy storage density while discharging ( $W_d$ ), energy density ( $W$ ), and the efficiency ( $\eta$ ). The above equations give the relationship between the three mentioned quantities[47]. The addition of Er<sup>3+</sup> ions as dopants to KNN ceramic has been observed to enhance the energy storage efficiency, particularly under moderate electric fields. Calculations revealed that undoped

KNN ceramic ( $x = 0$ ) had energy storage values ( $W$ ,  $W_d$ , and  $\eta$ ) of  $0.352 \text{ J/cm}^3$ ,  $0.184 \text{ J/cm}^3$ , and  $52.27\%$  respectively. Conversely, for optimally doped KNN ceramic ( $x = 3$ ), the corresponding values were  $0.302 \text{ J/cm}^3$ ,  $0.203 \text{ J/cm}^3$ , and  $67.21\%$ . These findings indicate the potential of  $\text{Er}^{3+}$ -doped KNN ceramic for application in optoelectronic devices.

## CHAPTER 4

### CONCLUSION

The investigation focuses on the impact of incorporating the rare earth element Erbium ( $\text{Er}^{3+}$ ) into the lead-free ceramic potassium sodium niobate ( $\text{K}_{0.5}\text{Na}_{0.5}\text{NbO}_3$ ), abbreviated as KNN: xEr (where  $x = 0, 1, 2, 3,$  and  $4$ ). The study aims to analyze the influence of  $\text{Er}^{3+}$  ions on the structural, ferroelectric, and photoluminescence properties of the material. The synthesis of KNN: xEr involves the solid-state method.

To obtain a well-defined perovskite crystal phase with an orthorhombic crystal structure, the undoped KNN is subjected to a gradual calcination process, starting from  $700^\circ\text{C}$  and incrementally increasing the temperature up to  $900^\circ\text{C}$ . Subsequently, the calcined material is sintered at a temperature of  $1100^\circ\text{C}$  for a duration of 3 hours. The absence of any additional phases in the X-ray diffraction (XRD) spectra of the  $\text{Er}^{3+}$ -enriched KNN indicates that all the  $\text{Er}^{3+}$  ions have successfully integrated into the host lattice.

The FTIR spectrum analysis revealed the presence of characteristic peaks at approximately  $486\text{ cm}^{-1}$  and  $720\text{ cm}^{-1}$ , indicating the development of a perovskite structure in the studied materials. To further investigate the photoluminescence (PL) properties of the  $\text{Er}^{3+}$ -doped KNN particles, emission spectra were measured at room temperature using two different excitation wavelengths:  $488\text{ nm}$  and  $980\text{ nm}$ .

Under both excitation conditions, the emission spectra exhibited intense green bands at approximately  $528\text{ nm}$  and  $549\text{ nm}$ , as well as less intense red bands at around  $662\text{ nm}$ . The emission intensity was found to be significantly higher in the upconversion PL spectra compared to the downconversion PL spectra when excited at  $980\text{ nm}$ . This observation suggests that the emission process in these ceramics involves a two-photon pumping mechanism.

Furthermore, the influence of pump strength on the emission process was examined, leading to the determination that ceramics utilize a two-photon pumping process for their

emission. The results indicate that the upconversion PL spectra exhibited greater emission intensity compared to the vis-down conversion PL when excited at 980 nm.

The ferroelectric properties of both the doped and undoped KNN ceramic were assessed, and satisfactory results were obtained. At room temperature, the ferroelectric polarization-electric field (PE) loops exhibited good loop shapes, indicating favorable ferroelectric behavior. Additionally, the remnant polarization of the doped and undoped KNN ceramic was found to be at a satisfactory level.

Furthermore, the energy storage capabilities of the KNN ceramic were significantly enhanced through the introduction of rare earth doping. The energy storage efficiency ( $\eta$ ) of the undoped KNN ( $x = 0$ ) ceramics was observed to be 52.27%. However, with the optimal  $\text{Er}^{3+}$  content ( $x = 3$ ), the efficiency improved to 67.21%. This improvement signifies the enhanced energy storage potential of the doped KNN ceramic.

Notably, this type of material possesses inherent piezoelectric capabilities, which are highly desirable. Moreover, by combining its optical and ferroelectric properties, the doped KNN ceramic demonstrates the potential to be utilized as a multifunctional optoelectronic device.

## REFERENCES

- [1] R. Capelletti, "Luminescence," *Reference Module in Materials Science and Materials Engineering*, Jan. 2017, doi: 10.1016/B978-0-12-803581-8.01247-9.
- [2] N. Hussain *et al.*, "Introduction to phosphors and luminescence," *Rare-Earth-Activated Phosphors: Chemistry and Applications*, pp. 3–41, Jan. 2022, doi: 10.1016/B978-0-323-89856-0.00008-0.
- [3] B. P. Kafle, "Molecular luminescence spectroscopy," *Chemical Analysis and Material Characterization by Spectrophotometry*, pp. 269–296, Jan. 2020, doi: 10.1016/B978-0-12-814866-2.00009-9.
- [4] W. U. Xiao, "RARE-EARTH-DOPED KNN-BASED CERAMICS FOR PHOTOLUMINESCENT AND ELECTRO-OPTIC APPLICATIONS."
- [5] A. Jain and S. J. Dhoble, "Upconversion luminescence behavior of rare-earth-activated phosphors: journey of infrared to visible," *Rare-Earth-Activated Phosphors: Chemistry and Applications*, pp. 291–308, Jan. 2022, doi: 10.1016/B978-0-323-89856-0.00016-X.
- [6] J. C. Goldschmidt and S. Fischer, "Upconversion for photovoltaics - a review of materials, devices and concepts for performance enhancement," *Adv. Opt. Mater.*, vol. 3, no. 4. Wiley-VCH Verlag, pp. 510–535, Apr. 01, 2015. doi: 10.1002/adom.201500024.
- [7] A. Pirri, G. Toci, B. Patrizi, and M. Vannini, "An overview on yb-doped transparent polycrystalline sesquioxide laser ceramics," *J. Sel. Top. Quantum Electron.*, vol. 24, no. 5, Sep. 2018, doi: 10.1109/JSTQE.2018.2799003.
- [8] H. Wei *et al.*, "An overview of lead-free piezoelectric materials and devices," *Journal of Materials Chemistry C*, vol. 6, no. 46. RSC, pp. 12446–12467, 2018. doi: 10.1039/c8tc04515a.
- [9] E. Shafiee, M. D. Chermahini, A. Doostmohammadi, M. R. Nilforoushan, and B. Zehipour, "Influence of sintering temperature on densification, microstructure, dielectric and ferroelectric properties of Li/Sb Co-doped KNN piezoceramics," *Ceram Int*, vol. 45, no. 17, pp. 22203–22206, Dec. 2019, doi: 10.1016/j.ceramint.2019.07.242.
- [10] A. Rahman *et al.*, "Improved ferroelectric, piezoelectric, and dielectric properties in pure KNN translucent ceramics by optimizing the normal sintering method," *Ceram Int*, vol. 48, no. 14, pp. 20251–20259, Jul. 2022, doi: 10.1016/j.ceramint.2022.03.305.
- [11] Z. Dai *et al.*, "A strategy for high performance of energy storage and transparency in KNN-based ferroelectric ceramics," *Chem. Eng. J.*, vol. 427, Jan. 2022, doi: 10.1016/j.cej.2021.131959.
- [12] A. Rajasri, N. V. Prasad, G. Prasad, and G. S. Kumar, "Synthesis and DC conductivity studies of multivalent substituted ABO<sub>3</sub> perovskite KNN multifunctional ferroelectric materials," in *Mater. Today Proc.*, Elsevier Ltd, 2019, pp. 1061–1065. doi: 10.1016/j.matpr.2018.12.039.
- [13] B. C. Park, I. K. Hong, H. D. Jang, V. D. N. Tran, W. P. Tai, and J. S. Lee, "Highly enhanced mechanical quality factor in lead-free (K<sub>0.5</sub>Na<sub>0.5</sub>)NbO<sub>3</sub> piezoelectric ceramics by co-

- doping with  $K_{5.4}Cu_{1.3}Ta_{10}O_{29}$  and  $CuO$ ,” *Mater Lett*, vol. 64, no. 14, pp. 1577–1579, Jul. 2010, doi: 10.1016/J.MATLET.2010.04.031.
- [14] S. Kawada, M. Kimura, Y. Higuchi, and H. Takagi, “(KNa)NbO<sub>3</sub>-Based multilayer piezoelectric ceramics with nickel inner electrodes,” *APEX*, vol. 2, no. 11, p. 111401, Nov. 2009, doi: 10.1143/APEX.2.111401/XML.
- [15] F. Z. Yao, E. A. Patterson, K. Wang, W. Jo, J. Rödel, and J. F. Li, “Enhanced bipolar fatigue resistance in CaZrO<sub>3</sub>-modified (K,Na)NbO<sub>3</sub> lead-free piezoceramics,” *Appl Phys Lett*, vol. 104, no. 24, Jun. 2014, doi: 10.1063/1.4884826/384933.
- [16] F. Z. Yao, K. Wang, Y. Shen, and J. F. Li, “Robust CaZrO<sub>3</sub>-modified (K, Na)NbO<sub>3</sub>-based lead-free piezoceramics: High fatigue resistance insensitive to temperature and electric field,” *J Appl Phys*, vol. 118, no. 13, Oct. 2015, doi: 10.1063/1.4932144/140203.
- [17] J. Rödel, K. G. Webber, R. Dittmer, W. Jo, M. Kimura, and D. Damjanovic, “Transferring lead-free piezoelectric ceramics into application,” *J Eur Ceram Soc*, vol. 35, no. 6, pp. 1659–1681, Jun. 2015, doi: 10.1016/J.JEURCERAMSOC.2014.12.013.
- [18] C.-H. Hong *et al.*, “Ring-Type Rotary Ultrasonic Motor Using Lead-free Ceramics,” *Journal of Sensor Science and Technology*, vol. 24, no. 4, pp. 228–231, Jul. 2015, doi: 10.5369/JSST.2015.24.4.228.
- [19] K. Kobayashi, Y. Doshida, Y. Mizuno, and C. A. Randall, “Possibility of cofiring a nickel inner electrode in a (Na<sub>0.5</sub>K<sub>0.5</sub>)NbO<sub>3</sub>-LiF piezoelectric actuator,” *Jpn J Appl Phys*, vol. 52, no. 9 PART2, p. 09KD07, Sep. 2013, doi: 10.7567/JJAP.52.09KD07/XML.
- [20] M. Guo *et al.*, “A Rosen-type piezoelectric transformer employing lead-free K<sub>0.5</sub>Na<sub>0.5</sub>NbO<sub>3</sub> ceramics,” *J Mater Sci*, vol. 43, no. 2, pp. 709–714, Jan. 2008, doi: 10.1007/S10853-007-2199-0/METRICS.
- [21] B. Malič *et al.*, “Sintering of lead-free piezoelectric sodium potassium niobate ceramics,” *Materials*, vol. 8, no. 12. MDPI AG, pp. 8117–8146, 2015. doi: 10.3390/ma8125449.
- [22] J. Acker, H. Kungl, and M. J. Hoffmann, “Influence of Alkaline and Niobium Excess on Sintering and Microstructure of Sodium-Potassium Niobate (K<sub>0.5</sub>Na<sub>0.5</sub>)NbO<sub>3</sub>,” *J. Am. Ceram. Soc.*, vol. 93, no. 5, pp. 1270–1281, May 2010, doi: 10.1111/J.1551-2916.2010.03578.X.
- [23] H. C. Thong *et al.*, “Technology transfer of lead-free (K, Na)NbO<sub>3</sub>-based piezoelectric ceramics,” *Mater. Today*, vol. 29. Elsevier B.V., pp. 37–48, Oct. 01, 2019. doi: 10.1016/j.mattod.2019.04.016.
- [24] S. Bairagi and S. W. Ali, “Effects of surface modification on electrical properties of KNN nanorod-incorporated PVDF composites,” *J Mater Sci*, vol. 54, no. 17, pp. 11462–11484, Sep. 2019, doi: 10.1007/s10853-019-03719-x.
- [25] M. S. El-Eskandarany, “Mechanically induced solid state reduction,” in *Mechanical Alloying*, Elsevier, 2015, pp. 132–151. doi: 10.1016/B978-1-4557-7752-5.00006-1.
- [26] A. Banwal and R. Bokolia, “Phase evolution and microstructure of BaBi<sub>2</sub>Nb<sub>2</sub>O<sub>9</sub> ferroelectric ceramics,” in *Mater. Today Proc.*, Elsevier Ltd, 2021, pp. 10121–10124. doi: 10.1016/j.matpr.2020.09.380.

- [27] A. Dahiya, O. P. Thakur, and J. K. Juneja, "Sensing and actuating applications of potassium sodium niobate: Use of potassium sodium niobate in sensor and actuator," in *Proceedings of the International Conference on Sensing Technology, ICST*, 2013, pp. 383–386. doi: 10.1109/ICSensT.2013.6727680.
- [28] Q. Jin, M. Jiang, S. Han, and Y. Yan, "Microstructure, optical and electrical properties of Bi and Ba co-doped  $K_{0.52}Na_{0.48}NbO_3$  transparent ceramics," *J. Mater. Sci. Mater. Electron.*, vol. 29, no. 15, pp. 13407–13417, Aug. 2018, doi: 10.1007/s10854-018-9466-5.
- [29] S. Dwivedi, T. Pareek, and S. Kumar, "Structure, dielectric, and piezoelectric properties of  $K_{0.5}Na_{0.5}NbO_3$ -based lead-free ceramics," *RSC Adv*, vol. 8, no. 43, pp. 24286–24296, 2018, doi: 10.1039/c8ra04038a.
- [30] X. Wu, C. M. Lau, and K. W. Kwok, "Effect of phase transition on photoluminescence of Er-doped KNN ceramics," *J Lumin*, vol. 155, pp. 343–350, 2014, doi: 10.1016/j.jlumin.2014.07.005.
- [31] A. Banwal and R. Bokolia, "Enhanced upconversion luminescence and optical temperature sensing performance in  $Er^{3+}$  doped  $BaBi_2Nb_2O_9$  ferroelectric ceramic," *Ceram Int*, vol. 48, no. 2, pp. 2230–2240, Jan. 2022, doi: 10.1016/J.CERAMINT.2021.09.314.
- [32] A. Banwal and R. Bokolia, "Effect of  $Er^{3+}$  ion doping on structural, ferroelectric and up/down conversion luminescence in  $BaBi_2Nb_2O_9$  ceramic," *Mater Today Proc*, vol. 47, pp. 4692–4695, Jan. 2021, doi: 10.1016/J.MATPR.2021.05.545.
- [33] W. Li *et al.*, "Optical temperature sensing properties and thermoluminescence behavior in Er-modified potassium sodium niobate-based multifunctional ferroelectric ceramics," *J Mater Chem C Mater*, vol. 10, no. 33, pp. 11891–11902, Jun. 2022, doi: 10.1039/d2tc01268e.
- [34] D. Peng *et al.*, "Upconversion luminescence, ferroelectrics and piezoelectrics of Er Doped  $SrBi_4Ti_4O_{15}$ ," *AIP Adv*, vol. 2, no. 4, Dec. 2012, doi: 10.1063/1.4773318.
- [35] W. Li, Z. Xu, R. Chu, P. Fu, and G. Zang, "Improved piezoelectric property and bright upconversion luminescence in Er doped  $(Ba_{0.99}Ca_{0.01})(Ti_{0.98}Zr_{0.02})O_3$  ceramics," *J Alloys Compd*, vol. 583, pp. 305–308, 2014, doi: 10.1016/j.jallcom.2013.08.103.
- [36] Z. Cao, J. Wang, C. Zhang, X. Mao, and L. Luo, "Flexible piezoelectric nanogenerator based on the  $Er^{3+}$  doped lead-free  $(Na_{0.5}Bi_{0.5})TiO_3$ - $BaTiO_3$  piezoelectric nanofibers with strong upconversion luminescence," *J Alloys Compd*, vol. 918, Oct. 2022, doi: 10.1016/j.jallcom.2022.165766.
- [37] H. Liu, J. Wang, H. Wang, J. Xu, C. Zhou, and W. Qiu, " $Er^{3+}$  and  $Sr(Bi_{0.5}Nb_{0.5})O_3$ -modified  $(K_{0.5}Na_{0.5})NbO_3$ : A new transparent fluorescent ferroelectric ceramic with high light transmittance and good luminescence performance," *Ceram Int*, vol. 48, no. 3, pp. 4230–4237, Feb. 2022, doi: 10.1016/j.ceramint.2021.10.215.
- [38] R. Bokolia, O. P. Thakur, V. K. Rai, S. K. Sharma, and K. Sreenivas, "Dielectric, ferroelectric and photoluminescence properties of  $Er^{3+}$  doped  $Bi_4Ti_3O_{12}$  ferroelectric ceramics," *Ceram Int*, vol. 41, no. 4, pp. 6055–6066, May 2015, doi: 10.1016/j.ceramint.2015.01.062.


- [39] M. K. Mahata *et al.*, "Incorporation of Zn<sup>2+</sup> ions into BaTiO<sub>3</sub>:Er<sup>3+</sup>/Yb<sup>3+</sup> nanophosphor: An effective way to enhance upconversion, defect luminescence and temperature sensing," *Phys. Chem. Chem. Phys.*, vol. 17, no. 32, pp. 20741–20753, Aug. 2015, doi: 10.1039/c5cp01874a.
- [40] D. Baziulyte-Paulaviciene, N. Traskina, R. Vargalis, A. Katelnikovas, and S. Sakirzanovas, "Thermal decomposition synthesis of Er<sup>3+</sup>-activated NaYbF<sub>4</sub> upconverting microparticles for optical temperature sensing," *J Lumin*, vol. 215, Nov. 2019, doi: 10.1016/j.jlumin.2019.116672.
- [41] R. Bokolia, O. P. Thakur, V. K. Rai, S. K. Sharma, and K. Sreenivas, "Electrical properties and light up conversion effects in Bi<sub>3.79</sub>Er<sub>0.03</sub>Yb<sub>0.18</sub>Ti<sub>3-x</sub>W<sub>x</sub>O<sub>12</sub> ferroelectric ceramics," *Ceram Int*, vol. 42, no. 5, pp. 5718–5730, Apr. 2016, doi: 10.1016/j.ceramint.2015.12.103.
- [42] A. Banwal and R. Bokolia, "Thermometric sensing performance in Erbium modified SrBi<sub>2-x</sub>Nb<sub>2</sub>Er<sub>x</sub>O<sub>9</sub> ferroelectric ceramic for optoelectronic devices," *Ceram Int*, vol. 48, no. 23, pp. 34405–34414, Dec. 2022, doi: 10.1016/j.ceramint.2022.08.019.
- [43] Q. Zhang, K. Chen, L. Wang, H. Sun, X. Wang, and X. Hao, "A highly efficient, orange light-emitting (K<sub>0.5</sub>Na<sub>0.5</sub>)NbO<sub>3</sub>:Sm<sup>3+</sup>/Zr<sup>4+</sup> lead-free piezoelectric material with superior water resistance behavior," *J Mater Chem C Mater*, vol. 3, no. 20, pp. 5275–5284, May 2015, doi: 10.1039/c4tc02995j.
- [44] S. Kumar and N. Thakur, "Effect of alkali metal (Na, K) ion ratio on structural, optical and photoluminescence properties of K<sub>0.5</sub>Na<sub>0.5</sub>NbO<sub>3</sub> ceramics prepared by sol-gel technique," *Bull. Mater. Sci.*, vol. 44, no. 1, 2021, doi: 10.1007/s12034-020-02341-x.
- [45] A. Banwal and R. Bokolia, "Preparation and characterisations of Yb<sup>3+</sup> substituted BaBi<sub>2-y</sub>Nb<sub>2</sub>Yb<sub>y</sub>O<sub>9</sub> ferroelectric ceramic," *Mater Today Proc*, vol. 62, pp. 3782–3785, Jan. 2022, doi: 10.1016/J.MATPR.2022.04.459.
- [46] Y. A. Genenko, J. Glaum, M. J. Hoffmann, and K. Albe, "Mechanisms of aging and fatigue in ferroelectrics," *Mater. Sci. Eng. B*, vol. 192, no. C. Elsevier Ltd, pp. 52–82, Feb. 01, 2015. doi: 10.1016/j.mseb.2014.10.003.
- [47] J. Zhang, Y. Lin, L. Wang, Y. Yang, H. Yang, and Q. Yuan, "Significantly enhanced energy storage density in sodium bismuth titanate-based ferroelectrics under low electric fields," *J Eur Ceram Soc*, vol. 40, no. 15, pp. 5458–5465, Dec. 2020, doi: 10.1016/j.jeurceramsoc.2020.06.059.



# Appendices

## Appendix 1: Plagiarism report

## Appendix 2: Registration Record



VIT  
AMARAVATI  
www.vitap.ac.in

**success**

Application Number	Participant Name	Amount Paid	Transaction Number	Status	Date Of Payment
NSFD220040	Shreya Soni	500	AMR2200012903	success	Mon Dec 05 10:29:42 IST 2022



DTU  
Delhi Technological  
UNIVERSITY

Shreya soni 2K21/MSCPHY/44 <shreyasoni\_2k21mscphy44@dtu.ac.in>

---

**Payment Info**  
1 message

---

**noreply.sdc@vitap.ac.in** <noreply.sdc@vitap.ac.in> Mon, Dec 5, 2022 at 10:30 AM  
To: shreyasoni\_2k21mscphy44@dtu.ac.in

**Dear Shreya Soni**

Greetings from NATIONAL SEMINAR ON FERROELECTRICS AND DIELECTRICS-22 (NSFD - 22). you have successfully registered .We have received your online payment of Rs 500 as Registration fee for NATIONAL SEMINAR ON FERROELECTRICS AND DIELECTRICS-22 (NSFD - 22). Your Application Number is NSFD220040 Please save this email for future reference.:  
This is an auto generated mail. Kindly don't reply or send message to this mail id.

VIT-AP.  
Amaravati -52237  
Andhra pradesh.  
SDC-Team.

## Appendix 3: Conference Presentation Record





Shreya soni 2K21/MSCPHY/44 <shreyasoni\_2k21mscphy44@dtu.ac.in>

---

**Acceptance of your abstract for NSFD-2022 (Online)**  
1 message

---

**nsfd.2022@vitap.ac.in** <nsfd.2022@vitap.ac.in> Sun, Nov 27, 2022 at 1:33 AM  
To: shreyasoni\_2k21mscphy44@dtu.ac.in

Dear Ms. Shreya Soni  
Thank you for submitting the abstract of your research work to participate in NSFD-2022 (Online). We are pleased to inform you that your abstract with the title "Modification of structural, ferroelectric and photoluminescence properties of KNN by Er3+ incorporation" has been accepted for **Oral Presentation**.  
Your abstract ID is: 22120606  
Kindly complete the registration process by 5th December 2022.  
Keep your application number that you receive to your email id in the registration process, and the abstract id for future reference.  
The details regarding your presentation will be communicated shortly.

You are encouraged to submit the full length paper after presenting it in the conference. The Template of the paper / guidelines for submitting the paper will be communicated soon. All the presented full length papers will be forwarded to the Journal "Ferroelectrics" and the papers accepted by the reviewers will be published in the journal.

Thanks and Regards  
Convener  
NSFD-2022

## Appendix 4: Status of Journal Paper

em Ceramics International Muskan Varshney | Logout

Home Main Menu Submit a Manuscript About Help

← Submissions Being Processed for Author ⓘ

Page: 1 of 1 (1 total submissions) Results per page 10

Action	Manuscript Number	Title	Authorship	Initial Date Submitted	Status Date	Current Status
Action Links	CERI-D-23-05247	Energy storage capacity and bight upconversion luminescence studies in Er <sup>3+</sup> modified K <sub>0.5</sub> Na <sub>0.5</sub> NbO <sub>3</sub> ceramics	Other Author	Apr 27, 2023	May 08, 2023	Under Review

Page: 1 of 1 (1 total submissions) Results per page 10 ⓘ

### Reviewers:

Suggested Reviewers:	Dr. Manoj Verma mverma@hinducollege.du.ac.in
	Dr. Geeta Rani geeta.rani@mirandahouse.ac.in
	Dr. M. Boazbou Newmai gingermax7@gmail.com

## Appendix 5: Manuscript Draft

**Ceramics International**  
**Energy storage capacity and bight upconversion luminescence studies in Er<sup>3+</sup>**  
**modified K<sub>0.5</sub>Na<sub>0.5</sub>NbO<sub>3</sub> ceramics**  
 --Manuscript Draft--

<b>Manuscript Number:</b>	CERI-D-23-05247
<b>Article Type:</b>	Full length article
<b>Keywords:</b>	Photoluminescence; ferroelectrics; Energy storage; upconversion; hysteresis loop; XRD spectra
<b>Corresponding Author:</b>	RENUKA BOKOLIA, Ph.D. Delhi Technological University Department of Applied Physics INDIA
<b>First Author:</b>	Muskan Varshney
<b>Order of Authors:</b>	Muskan Varshney Shreya Soni Ankita Banwal RENUKA BOKOLIA, Ph.D.
<b>Abstract:</b>	The lead-free ceramics potassium sodium niobate doped with the rare earth element, Er <sup>3+</sup> , i.e., K <sub>0.5</sub> Na <sub>0.5</sub> NbO <sub>3</sub> : x wt% Er <sup>3+</sup> (x = 0, 1, 2, 3 and 4) were produced through the solid-state technique so that the impact of Er <sup>3+</sup> on structural, ferroelectric and optical properties can be studied. The undoped K <sub>0.5</sub> Na <sub>0.5</sub> NbO <sub>3</sub> (KNN) was calcined from 700°C to 900°C and finally sintered at 1100°C for three hours to produce a pure-phase perovskite with an orthorhombic structure. The absence of extra phases in the XRD spectra of Er <sup>3+</sup> enriched KNN demonstrates that all the Er <sup>3+</sup> ions have dispersed into the host lattice. The FTIR band observed near 486 cm <sup>-1</sup> and 720 cm <sup>-1</sup> showed the formation of a perovskite structure. At room temperature, the photoluminescence (PL) emission spectra of sintered Er <sup>3+</sup> modified KNN pellets were examined in response to excitation wavelength of 488 nm and 980 nm. In both emission spectra, prominent green emission bands (528 nm and 549 nm) and slightly faint red emission bands (662 nm) were found. The upconversion PL spectra observed at 980 nm excitation showed a much higher emission intensity than the vis-down conversion PL. Observing the effect of pump power revealed that two photons are involved in the emission process. Time decay profile associated with the 4S <sub>3/2</sub> → 4I <sub>15/2</sub> level indicates an average lifetime of Er <sup>3+</sup> ions is 25.05µs. The ferroelectric hysteresis loop at room temperature showed decent shapes with good remnant polarization for doped KNN ceramic. In addition, rare earth modification has enhanced the energy storage capacities of the KNN ceramic. The efficacy of undoped KNN is calculated to be 52.27 %, while the efficiency of optimum Er <sup>3+</sup> doped KNN is calculated to be 67.2 %. Thus, by combining the optical and ferroelectric properties, KNN may have potential applications to be employed in optoelectronic devices.
<b>Suggested Reviewers:</b>	Dr. Manoj Verma mverma@hinducollege.du.ac.in  Dr. Geeta Rani geeta.rani@mirandahouse.ac.in  Dr. M. Boazbou Newmai gingermax7@gmail.com
<b>Opposed Reviewers:</b>	

## Appendix 6: Index of Journal

The screenshot shows the journal's homepage on ScienceDirect. At the top, the ScienceDirect logo is on the left, and navigation links for 'Journals & Books', a search icon, and a user profile for 'Muskan Varshney' are on the right. The user profile also indicates they are 'Brought to you by: Delhi College of Engineering'. Below the navigation bar, the journal's cover image is on the left, and the journal title 'Ceramics International' is prominently displayed in the center. To the right of the title, the journal's CiteScore (8) and Impact Factor (5.532) are shown. A dark blue navigation bar contains links for 'Articles & Issues', 'About', 'Publish', a search bar, 'Submit your article', and 'Guide for authors'. The main content area is divided into two sections: 'Latest issue' on the left, which highlights 'Volume 49, Issue 12' dated '15 June 2023', and 'About the journal' on the right, which provides a brief description of the journal's focus on advanced ceramic materials. A 'FEEDBACK' button is located at the bottom right of the 'About the journal' section.

ScienceDirect Journals & Books Muskan Varshney MV Brought to you by: Delhi College of Engineering

CERAMICS INTERNATIONAL

**Ceramics International**  
Supports open access

8 CiteScore | 5.532 Impact Factor

Articles & Issues About Publish Search in this journal Submit your article Guide for authors

Latest issue

**Volume 49, Issue 12**  
15 June 2023

**About the journal**

*Ceramics International* covers the science of advanced ceramic materials. The journal encourages contributions that demonstrate how an understanding of the basic chemical and physical phenomena may direct materials design and stimulate ideas for new or improved processing techniques, in order to ...

FEEDBACK